NASA TN D-232

TECHNICAL NOTE

D - 232

EXPERIMENTAL DETERMINATION

OF THE EFFECTS OF FREQUENCY AND AMPLITUDE OF OSCILLATION

ON THE ROLL-STABILITY DERIVATIVES FOR A

60° DELTA-WING AIRPLANE MODEL

By Lewis R. Fisher

Langley Research Center
Langley Field, Va.

NATIONAL AERONAUTICS AND SPACE ADMINISTRATION

WASHINGTON March 1960

NATIONAL AERONAUTICS AND SPACE ADMINISTRATION

TECHNICAL NOTE D-232

EXPERIMENTAL DETERMINATION OF THE EFFECTS OF FREQUENCY AND AMPLITUDE OF OSCILLATION ON THE ROLL-STABILITY DERIVATIVES FOR A 60° DELTA-WING AIRPLANE MODEL*

By Lewis R. Fisher

SUMMARY

A 60° delta-wing airplane model was oscillated in roll for several frequencies and amplitudes of oscillation to determine the effects of the oscillatory motion on the roll-stability derivatives for the model. The derivatives were measured at a Reynolds number of 1,600,000 for the wing alone, the wing-fuselage combination, and the complete model which included a triangular-plan-form vertical tail.

Both rolling and yawing moments due to rolling velocity exhibited large frequency effects for angles of attack higher than 16°. The largest variations in these derivatives were measured for the lowest frequencies of oscillation; as the frequency increased, the derivatives became more nearly linear with angle of attack. Both velocity derivatives were considerably different at high angles of attack from the corresponding derivatives measured by the steady-state rolling-flow technique.

Rolling and yawing moments due to rolling acceleration were measured and similarly found to be highly dependent on frequency at high angles of attack. Some period and time-to-damp computations, which were made to reveal the significance of the acceleration derivatives, indicated that inclusion of the measured derivatives in the equations of motion lengthened the period of the lateral oscillation by 10 percent for a typical delta-wing airplane and increased the time to damp to one-half amplitude by 50 percent.

---

*Supersedes recently declassified NACA Research Memorandum L57L17 by Lewis R. Fisher, 1958.

INTRODUCTION

The results of several experimental investigations (refs. 1 to 3) have demonstrated that large-magnitude lateral-stability derivatives may exist under oscillatory conditions for delta- and sweptback-plan-form wings and that at high angles of attack these oscillatory derivatives may be much different from those measured under steady-flow conditions. The stability derivatives which have been measured by oscillation tests are those which determine the directional stability, $C_{n_{\beta,\omega}}$ and $C_{n_{\dot{r},\omega}}$, and those which determine the damping in yaw, $C_{n_{r,\omega}}$ and $C_{n_{\dot{\beta},\omega}}$. These derivatives have been measured individually by oscillating the models with a sideslipping motion (ref. 1) or a yawing motion (ref. 2), and in combination by oscillating the models in yaw about their vertical axes (ref. 3).

Because the sideslipping and yawing derivatives of certain configurations are affected to a large degree by the frequency and amplitude of an oscillatory motion, it would seem likely that the phenomena which produce these results would affect the roll-stability derivatives in a like manner. A preliminary investigation in this area is reported in reference 4, for which an unswept-wing airplane model was oscillated in roll primarily at zero angle of attack. Certain of the higher angle-of-attack data in reference 4 gave an indication that differences do exist between the oscillatory and the steady-state rolling derivatives.

In the present investigation, an airplane model with a 60° delta wing was oscillated in roll about its longitudinal stability axis for several frequencies and amplitudes of oscillation in order to measure the effects of oscillatory motion on the roll-stability derivatives of the model. For a basis of comparison, the model was also tested in steady rolling flow, the resulting data being regarded as zero frequency data. The tests were made for the complete model, for the wing-fuselage combination, and for the wing alone at a Reynolds number of 1,600,000.

SYMBOLS

The data are referred to the stability system of axes (fig. 1) and are presented in the form of coefficients of the forces and moments about a point which is the projection of the quarter-chord location of the wing mean aerodynamic chord on the plane of symmetry. The coefficients and symbols used herein are defined as follows:

b wing span, ft

C_D drag coefficient, $\frac{\text{Drag}}{qS}$

C_L lift coefficient, $\frac{\text{Lift}}{qS}$

C_l rolling-moment coefficient, $\frac{\text{Rolling moment}}{qSb}$

$$C_{l_p} = \frac{\partial C_{l,s}}{\partial\left(\frac{pb}{2V}\right)}$$

$$C_{l_{\dot{p}}} = \frac{\partial C_{l,s}}{\partial\left(\frac{\dot{p}b^2}{4V^2}\right)}$$

$$C_{l_r} = \frac{\partial C_l}{\partial\left(\frac{rb}{2V}\right)}$$

$C_{l,s}$ rolling-moment coefficient, $\frac{M_{Xs}}{qSb}$

$$C_{l_\beta} = \frac{\partial C_l}{\partial \beta}$$

C_m pitching-moment coefficient, $\frac{M_{Ys}}{qS\bar{c}}$

C_n yawing-moment coefficient, $\frac{\text{Yawing moment}}{qSb}$

$$C_{n_p} = \frac{\partial C_{n,w}}{\partial\left(\frac{pb}{2V}\right)}$$

$$C_{n_{\dot{p}}} = \frac{\partial C_{n,w}}{\partial\left(\frac{\dot{p}b^2}{4V^2}\right)}$$

$C_{n_r} = \frac{\partial C_n}{\partial\left(\frac{rb}{2V}\right)}$

$C_{n_\beta} = \frac{\partial C_n}{\partial \beta}$

$C_{n,w}$ yawing-moment coefficient, $\frac{M_{Zs}}{qSb}$

C_Y lateral-force coefficient, $\frac{\text{Lateral force}}{qS}$

$C_{Y_p} = \frac{\partial C_Y}{\partial\left(\frac{pb}{2V}\right)}$

$C_{Y_r} = \frac{\partial C_Y}{\partial\left(\frac{rb}{2V}\right)}$

$C_{Y_\beta} = \frac{\partial C_Y}{\partial \beta}$

$\bar{c}$ mean aerodynamic chord, ft

d maximum diameter of fuselage, ft

F_Y lateral force, lb

f frequency, cps

h altitude, ft

K_X radius of gyration about X-axis, nondimensionalized with respect to b (ref. 5)

K_Z radius of gyration about Z-axis, nondimensionalized with respect to b (ref. 5)

K_{XZ} nondimensional product-of-inertia factor (ref. 5)

$k = \frac{\omega b}{2V}$

k_X	radius of gyration about X-axis, ft (ref. 5)
k_Z	radius of gyration about Z-axis, ft (ref. 5)
k_{XZ}	product-of-inertia factor (ref. 5)
M_{Xs}	rolling moment, ft-lb
M_{Xs_1}	rolling moment in phase with velocity of oscillation, ft-lb
M_{Xs_2}	rolling moment out of phase with velocity of oscillation, ft-lb
M_{Ys}	pitching moment, ft-lb
M_{Zs}	yawing moment, ft-lb
M_{Zs_1}	yawing moment in phase with velocity of oscillation, ft-lb
M_{Zs_2}	yawing moment out of phase with velocity of oscillation, ft-lb
m	mass of airplane, slugs
P	period of oscillation, sec
$p = \frac{d\phi}{dt}$	
$\dot{p} = \frac{d^2\phi}{dt^2}$	
q	dynamic pressure, $\frac{1}{2}\rho V^2$, lb/sq ft
r	yawing velocity, $\frac{d\psi}{dt}$, radians/sec
S	wing area, sq ft
$T_{1/2}$	time for oscillatory motion to damp to half-amplitude, sec
t	time, sec

V	free-stream velocity, ft/sec
v	lateral component of velocity, ft/sec
X,Y,Z	system of stability axes (fig. 1)
α	angle of attack, deg
β	angle of sideslip, radians except when otherwise indicated
γ	angle of flight path, deg (ref. 5)
η	angle of attack of principal longitudinal axis of inertia, deg (ref. 5)
μ	relative density factor, $m/\rho Sb$
ρ	mass density of air, slugs/cu ft
ϕ	angle of roll, deg or radians
ϕ_o	amplitude of oscillation, deg or radians
ψ	angle of yaw, radians

$\omega = 2\pi f$

The symbol ω following the subscript of a derivative denotes the oscillatory derivative; for example, $C_{l_{p,\omega}}$ is the oscillatory value of C_{l_p}.

APPARATUS

Oscillation Equipment

The tests were conducted in the 6-foot-diameter rolling-flow test section of the Langley stability tunnel. A motor-driven flywheel shown in figure 2 and mounted externally on the tunnel test section was used to oscillate the models. A connecting rod pinned to an eccentric center on the flywheel passed through a hole in the tunnel wall and transmitted an essentially sinusoidal motion to the model support sting by means of a crank arm attached to the sting. This equipment is shown in figures 2 and 3. The roll axis of the sting was alined at all times with the wind stream.

The apparatus was driven by a 1-horsepower direct-current motor through a geared speed reducer. The frequency of oscillation was varied by controlling the voltage supplied to the motor and the amplitude of oscillation was varied by adjusting the throw of the eccentric on the flywheel.

Model

The model tested had a triangular wing with a 60° apex angle, an aspect ratio of 2.31, and NACA 65A003 sections parallel to the plane of symmetry. The fuselage was a body of revolution which had a sharp nose and a truncated afterbody with the wing mounted at the midfuselage height. The fuselage contained a two-component wire strain-gage balance to which the model was mounted at the quarter-chord point of the wing mean aerodynamic chord. The model was also equipped with the triangular-planform vertical tail shown in figures 4 and 5. The entire model was constructed of balsa wood to minimize inertia moments during oscillation and was covered with a thin layer of fiberglass-reinforced plastic to provide strength. Additional geometric characteristics of the model are presented in table I.

Recording of Data

The model was mounted to the support sting by means of a resistance-type wire strain-gage balance which measured rolling and yawing moments. The strain-gage signals, during oscillation, were modified by a sine-cosine resolver driven by the oscillating mechanism so that the measured signals of the strain gages were proportional to the in-phase and out-of-phase components of the strain-gage moments. These signals were read visually on a highly damped direct-current galvanometer and the aerodynamic coefficients were obtained by multiplying the meter readings by the appropriate constants, one of which was the system calibration constant. This data recording system is described in detail in reference 2.

Steady Rolling-Flow Equipment

In order to measure the steady rolling derivatives, the model was supported by the same strain-gage balance and support sting as were used for the oscillation tests with the angle of roll fixed at zero. The air flow over the model, however, was forced to roll by a rotor placed in the airstream ahead of the model. This is the standard rolling-flow test procedure employed in the Langley stability tunnel and is described in reference 6. For these tests, the resolver in the data recording equipment was bypassed and the total strain-gage output signals were read directly from the galvanometer.

TESTS

Both the oscillation and the rolling-flow tests were made at a dynamic pressure of 24.9 pounds per square foot which corresponds to a free-stream velocity of 145 feet per second (under standard conditions), a Reynolds number of approximately 1,600,000 based on the wing mean aerodynamic chord, and a Mach number of 0.13.

The oscillation tests were made at frequencies of oscillation of 0.5, 1, 2, and 4 cycles per second, amplitudes of oscillation of $\pm 5^{\circ}$, $\pm 10^{\circ}$, and $\pm 20^{\circ}$, and angles of attack from 0° to 32°. The oscillation frequencies correspond to a range of the reduced-frequency parameter from $k = 0.033$ to $k = 0.264$. For certain combinations of the highest frequencies and amplitudes, the yawing moments due to the inertia of the model exceeded the maximum design moment of the strain-gage balance and, for this reason, tests for these conditions were not run. For all conditions of frequency, amplitude, and angle of attack both a wind-off and a wind-on run were made.

In order to establish the magnitude of the damping of the wing due to its rotation in still air, some tests were made in which the wing was enclosed in a plywood box. The box, which was mounted to the sting below the model support, was forced to rotate with the sting so that the volume of air immediately surrounding the wing was forced to oscillate with it. The still-air moments measured in this manner were found to be negligible and were not considered further.

The steady rolling-flow tests were conducted for the same model configuration and angles of attack as for the oscillation tests. The rotary helix angles of the air flow by the model during these tests corresponded to values of $pb/2V$ of 0.059, 0.033, 0.010, -0.021, -0.039, and -0.065.

REDUCTION OF DATA

Subtracting the wind-off data from the wind-on data in order to eliminate the effects of model inertia on the derivatives and then multiplying the results by the strain-gage balance calibration factors gives the in-phase moments M_{Xs_1} and M_{Zs_1} in foot-pounds and the out-of-phase moments M_{Xs_2} and M_{Zs_2} in foot-pounds. These moments were then reduced to coefficient derivative form by means of the following equations:

$$C_{l_{p,\omega}} = \frac{M_{X_{s_1}}}{qSbk\phi_o} \qquad C_{n_{p,\omega}} = \frac{M_{Z_{s_1}}}{qSbk\phi_o}$$

$$C_{l_{\dot{p},\omega}} = \frac{M_{X_{s_2}}}{qSbk^2\phi_o} \qquad C_{n_{\dot{p},\omega}} = \frac{M_{Z_{s_2}}}{qSbk^2\phi_o}$$

where the reduced-frequency parameter $\omega b/2V$ is represented by k.

The steady rolling derivatives were determined by plotting the moments as functions of $pb/2V$ and measuring the slopes of these curves.

PRESENTATION OF RESULTS

The static lift, drag, and pitching-moment coefficients for the wing, for the wing fuselage, and for the complete model are shown for reference in figure 6. In figure 7, the damping in roll $C_{l_{p,\omega}}$ measured during oscillation in roll is shown for the three configurations tested as a function of the nominal angle of attack for four values of reduced frequency and three amplitudes of oscillation. The corresponding steady rolling-flow values of C_{l_p} are also presented in figure 7. Figure 8 is a similar figure for the presentation of the oscillatory values of the yawing moment due to rolling velocity $C_{n_{p,\omega}}$ together with the steady rolling-flow derivative C_{n_p}.

Figures 9 and 10 present, respectively, the rolling moment due to rolling acceleration $C_{l_{\dot{p},\omega}}$ and the yawing moment due to rolling acceleration $C_{n_{\dot{p},\omega}}$. In the steady rolling-flow case, the acceleration derivatives are, of course, zero.

The oscillatory rolling derivatives are cross-plotted directly as functions of reduced frequency in figures 11 to 14 for three of the higher angles of attack. In these figures, the corresponding steady rolling-flow derivatives are shown as zero frequency values.

DISCUSSION

The Damping in Roll

The oscillatory damping in roll of the wing alone (fig. 7(a)) is shown to be largely dependent upon the frequency of oscillation for

angles of attack higher than 16°. The values of $C_{l_{p,\omega}}$ which become most positive are those measured for the lowest frequency of oscillation. With higher frequencies, the curves become more nearly linear with angle of attack. The derivative remains negative for all angles of attack for only the two highest frequencies, but even for these frequencies a considerable reduction in the damping (where positive damping is indicated by negative values of $C_{l_{p,\omega}}$) takes place between the two extremes in angle of attack. A change in the amplitude of oscillation from 5° to 20° produced generally small effects on the damping-in-roll results. (See also fig. 11(a).)

A notable difference exists between the oscillatory and the steady-state damping at high angles of attack. The steady-flow results indicate an increase in the damping as the angle of attack becomes large in contrast with the trends taken by the oscillation data. Similar differences between oscillatory and steady-state values of damping in yaw for a similar wing were observed in the investigation of reference 2.

The addition of the fuselage (figs. 7(b) and 11(b)) and of the fuselage and tail (figs. 7(c) and 11(c)) served to modify the large positive values of $C_{l_{p,\omega}}$ which were measured for the wing alone at the highest angles of attack. The effects of frequency on the damping for these configurations are in the same direction as for the wing alone but are not as large. Certain effects of amplitude of oscillation appeared for the wing-fuselage and the complete model configurations in that the values of the damping derivative measured for the lowest frequencies become more negative and the variations generally become more nearly linear with angle of attack as the amplitude becomes larger.

The Yawing Moment Due to Rolling Velocity

The initial slopes of $C_{n_{p,\omega}}$ and C_{n_p} at the low angles of attack for the wing (fig. 8(a)) and for the wing-fuselage configuration (fig. 8(b)) are small and positive. At angles of attack higher than 16°, the variations of the derivatives have trends in the negative direction in contrast with the steady-flow derivatives which become increasingly positive at the highest angles of attack. The most negative values of $C_{n_{p,\omega}}$ were measured for the lowest oscillation frequencies; as the frequency increased, the values became more positive and the curves more nearly linear with angle of attack. No particular effect of oscillation amplitude was evident for the wing-alone derivatives (fig. 12(a)); for the wing-fuselage combination, the higher amplitudes appear to make the lowest frequency data become more nearly positive and more linear with angle of attack (figs. 8(b) and 12(b)).

The addition of the vertical tail (fig. 8(c)) resulted in a substantial negative slope of $C_{n_{p,\omega}}$ and C_{n_p} with angle of attack at the low angles. The variation of C_{n_p} diverged in the positive direction beginning at about $\alpha = 20^\circ$ whereas those of $C_{n_{p,\omega}}$ remained relatively linear. The yawing-moment data for the complete model at the highest angle of attack includes a substantial amount of scatter because of the high degree of model buffeting which was present for this condition. The buffeting of the model was probably due to a combination of wing stall (see fig. 6) and an unsteady wake from the model support sting.

The Rolling Moment Due to Rolling Acceleration

A rolling moment which was out of phase with the rolling velocity was measured during the oscillation tests and was designated $C_{l_{\dot{p},\omega}}$. In general, this derivative has a small positive value up to an angle of attack of about 16° (fig. 9); thereafter, the derivative becomes more positive for the higher angles of attack particularly for the lowest frequencies of oscillation. An increase in frequency of oscillation decreases the magnitude of $C_{l_{\dot{p},\omega}}$ throughout the angle-of-attack range, the largest frequency effects taking place in the high angle range. The variation of $C_{l_{\dot{p},\omega}}$ with frequency shown for three angles of attack in figure 13 indicates that an increase in amplitude had an effect on the derivative only at the lowest frequencies of oscillation.

The Yawing Moment Due to Rolling Acceleration

The derivative $C_{n_{\dot{p},\omega}}$ remained generally small for the wing alone (fig. 10(a)) and the wing-fuselage (fig. 10(b)) at low angles of attack. At angles higher than about $\alpha = 16^\circ$, the derivative became increasingly negative with angle of attack for the low frequency of oscillation. At the higher frequencies for this angle-of-attack range, the effects of angle of attack were much smaller than those for the lowest frequency. The addition of the vertical tail results in magnitudes of $C_{n_{\dot{p},\omega}}$ which are relatively large, particularly for the highest frequency of oscillation. (See fig. 10(c).) These large-magnitude derivatives, which are positive at low angles of attack, are modified considerably and tend toward becoming negative at high angles of attack. The variations of $C_{n_{\dot{p},\omega}}$ with frequency, shown in figure 14, indicate that in the high angle range the measured values of the derivative for all configurations became increasingly negative as the frequency was reduced. For the model with the vertical tail, however, the opposite trend was shown at low

angles of attack. Increasing the amplitude of oscillation also generally resulted in somewhat more positive values of the derivative.

Significance of the $\dot{p}$ Derivatives

The existence of rolling and yawing moments due to rolling acceleration having been established in the preceding results, it is now of immediate interest to question the significance of these derivatives. A step in this direction was taken in this investigation by computing the period and damping of the lateral oscillation for a typical delta-wing airplane. The same airplane, whose aerodynamic, dimensional, and mass characteristics are given in table II, was the subject of some similar period and damping computations carried out for the investigation of reference 1. The equations of motion including the moments due to rolling acceleration and the resulting coefficients of the characteristic stability equation are given in the appendix. The steady-state stability derivatives used for these calculations were taken from references 7 and 8 and are listed in table II. Representative measured values of the derivatives $C_{l_{\dot{p},\omega}}$ and $C_{n_{\dot{p},\omega}}$ for an amplitude of $\pm 10^\circ$ were employed for several angles of attack from $\alpha = 2^\circ$ to $\alpha = 24^\circ$. The procedure followed was to compute the reduced frequency k based on the periods of oscillation for the airplane when the $\dot{p}$ derivatives were zero. Values of $C_{l_{\dot{p},\omega}}$ and $C_{n_{\dot{p},\omega}}$ were picked off the measured data curves similar to those of figures 13 and 14, respectively, for the proper value of the reduced frequency for each angle of attack. These values, which were used for the subsequent period and damping computations, are listed in table II.

The results of the computations (fig. 15) indicate that inclusion of the measured $C_{l_{\dot{p},\omega}}$ derivative alone in the equations of motion had a negligible effect on either the period of the lateral oscillation or the time to damp to one-half amplitude. Inclusion of the measured $C_{n_{\dot{p},\omega}}$ derivative, however, had a significant effect on the period and damping in that the length of the period was increased by roughly 10 percent and the time to damp to one-half amplitude was lengthened by roughly 50 percent over most of the angle-of-attack range. The inclusion of both derivatives simultaneously gave results which reflected the strong effect of $C_{n_{\dot{p},\omega}}$. The latter computation would indicate that the effects of the separate derivatives on the period and damping are additive. The relatively large effect of $C_{n_{\dot{p},\omega}}$ on the period and damping in contrast with the small effect of $C_{l_{\dot{p},\omega}}$ is probably due to the relative magnitudes of these derivatives. A glance at table II will show that the complete model configuration gave measured values of $C_{n_{\dot{p},\omega}}$ which were very large in comparison with the measured values of $C_{l_{\dot{p},\omega}}$.

CONCLUSIONS

An airplane model with a 60° delta wing was oscillated in roll for a range of frequencies and amplitudes of oscillation to measure the effects of the oscillatory motions on the roll-stability derivatives of the model. The conclusions drawn from the results of this investigation can be stated as follows:

1. For angles of attack lower than about 16°, the oscillatory damping in roll was generally in good agreement with the damping measured by means of steady rolling flow tests, and neither frequency nor amplitude of oscillation had any important effect on the magnitude of the damping. At the higher angles of attack, however, the oscillatory damping departed radically from the steady-state damping, the largest departures taking place for the lowest frequencies of oscillation. Although the steady-state results indicated some increase in damping at high angles of attack, the oscillatory damping decreased and in some instances changed sign.

2. The oscillation results exhibited trends for the yawing moment due to rolling that were similar to those for the damping in roll. At the high angles of attack the oscillatory derivative became more negative in contrast with the steady-state derivative which became more positive with increasing angle of attack. An increase in frequency reduced the differences between the oscillatory and steady-state data by making the oscillatory derivative more nearly linear with angle of attack.

3. Rolling and yawing moments in phase with the rolling acceleration were measured for the model and were also dependent on frequency at high angles of attack. The model with the vertical tail in particular showed relatively large values of the yawing moment due to rolling acceleration.

4. Some period and damping calculations, which were made to indicate the significance of the rolling acceleration derivatives, indicated that inclusion of the measured derivatives in the equations of motion lengthened the period of the lateral oscillation by 10 percent for a typical delta-wing airplane and increased the time to damp to one-half amplitude by 50 percent.

Langley Aeronautical Laboratory,
National Advisory Committee for Aeronautics,
Langley Field, Va., November 29, 1957.

APPENDIX

STABILITY CALCULATIONS

The stability roots were calculated from the lateral equations of motion:

Rolling moment:

$$mk_X^2 \frac{d^2\phi}{dt^2} - \frac{\partial M_{Xs}}{\partial \dot{p}} \frac{d^2\phi}{dt^2} - \frac{\partial M_{Xs}}{\partial p} \frac{d\phi}{dt} - mk_{XZ} \frac{d^2\psi}{dt^2} - \frac{\partial M_{Xs}}{\partial r} \frac{d\psi}{dt} - \frac{\partial M_{Xs}}{\partial v} v = 0$$

Yawing moment:

$$-mk_{XZ} \frac{d^2\phi}{dt^2} - \frac{\partial M_{Zs}}{\partial \dot{p}} \frac{d^2\phi}{dt^2} - \frac{\partial M_{Zs}}{\partial p} \frac{d\phi}{dt} + mk_Z^2 \frac{d^2\psi}{dt^2} - \frac{\partial M_{Zs}}{\partial r} \frac{d\psi}{dt} - \frac{\partial M_{Zs}}{\partial v} v = 0$$

Lateral force:

$$-\frac{\partial F_Y}{\partial p} \frac{d\phi}{dt} - (\text{Lift})\phi + mV\frac{d\psi}{dt} - \frac{\partial F_Y}{\partial r} \frac{d\psi}{dt} - (\text{Lift})(\tan \gamma)\psi + m\frac{dv}{dt} - \frac{\partial F_Y}{\partial v} v = 0$$

These equations are the same as those of reference 5 except for the addition of the $\frac{\partial M_{Xs}}{\partial \dot{p}}$ and $\frac{\partial M_{Zs}}{\partial \dot{p}}$ terms and a change in the sign of k_{XZ}. When reduced to nondimensional form, these equations become

$$2\mu\left(K_X^2 D^2\phi - K_{XZ} D^2\psi\right) = \tfrac{1}{2}C_{l_p} D\phi + \tfrac{1}{2}C_{l_r} D\psi + C_{l_\beta}\beta + \tfrac{1}{4}C_{l_{\dot{p}}} D^2\phi$$

$$2\mu\left(K_Z^2 D^2\psi - K_{XZ} D^2\phi\right) = \tfrac{1}{2}C_{n_r} D\psi + \tfrac{1}{2}C_{n_p} D\phi + C_{n_\beta}\beta + \tfrac{1}{4}C_{n_{\dot{p}}} D^2\phi$$

$$2\mu(D\beta + D\psi) = C_{Y_\beta}\beta + \tfrac{1}{2}C_{Y_p} D\phi + C_L\phi + \tfrac{1}{2}C_{Y_r} D\psi + \left(C_L \tan \gamma\right)\psi$$

From these equations, there follows the characteristic stability equation

$$A_1\lambda^4 + B_1\lambda^3 + C_1\lambda^2 + D_1\lambda + E_1 = 0$$

It can be shown that

$$A_1 = A - \mu^2\left(K_Z^2 C_{l_{\dot{p}}} + K_{XZ} C_{n_{\dot{p}}}\right)$$

$$B_1 = B + \frac{\mu}{4}\left[C_{l_{\dot{p}}}\left(C_{n_r} + 2K_Z^2 C_{Y_\beta}\right) - C_{n_{\dot{p}}}\left(C_{l_r} - 2K_{XZ}C_{Y_\beta}\right)\right]$$

$$C_1 = C + \frac{1}{8}\left\{C_{l_{\dot{p}}}\left[C_{n_\beta}\left(C_{Y_r} - 4\mu\right) - C_{Y_\beta}C_{n_r}\right] - C_{n_{\dot{p}}}\left[C_{l_\beta}\left(C_{Y_r} - 4\mu\right) - C_{Y_\beta}C_{l_r}\right]\right\}$$

$$D_1 = D$$

$$E_1 = E$$

The standard coefficients A, B, C, D, and E of the stability equation as defined, for example, in reference 9 are:

$$A = 8\mu^3\left(K_X^2 K_Z^2 - K_{XZ}^2\right)$$

$$B = -2\mu^2\left(2K_X^2 K_Z^2 C_{Y_\beta} + K_X^2 C_{n_r} + K_Z^2 C_{l_p} - 2K_{XZ}^2 C_{Y_\beta} - K_{XZ}C_{l_r} - K_{XZ}C_{n_p}\right)$$

$$C = \mu\left(K_X^2 C_{n_r}C_{Y_\beta} + 4\mu K_X^2 C_{n_\beta} + K_Z^2 C_{l_p}C_{Y_\beta} + \frac{1}{2}C_{n_r}C_{l_p} - K_{XZ}C_{l_r}C_{Y_\beta}\right.$$

$$\left. - 4\mu K_{XZ}C_{l_\beta} - C_{n_p}K_{XZ}C_{Y_\beta} - \frac{1}{2}C_{n_p}C_{l_r} + K_{XZ}C_{n_\beta}C_{Y_p} - K_Z^2 C_{Y_p}C_{l_\beta}\right.$$

$$\left. - K_X^2 C_{Y_r}C_{n_\beta} + K_{XZ}C_{Y_r}C_{l_\beta}\right)$$

$$D = -\frac{1}{4}C_{n_r}C_{l_p}C_{Y_\beta} - \mu C_{l_p}C_{n_\beta} + \frac{1}{4}C_{n_p}C_{l_r}C_{Y_\beta} + \mu C_{n_p}C_{l_\beta} + 2\mu C_L K_{XZ}C_{n_\beta}$$

$$- 2\mu C_L K_Z^2 C_{l_\beta} - 2\mu K_X^2 C_{n_\beta}C_L \tan\gamma + 2\mu K_{XZ}C_{l_\beta}C_L \tan\gamma + \frac{1}{4}C_{l_p}C_{n_\beta}C_{Y_r}$$

$$- \frac{1}{4}C_{n_p}C_{l_\beta}C_{Y_r} - \frac{1}{4}C_{l_r}C_{n_\beta}C_{Y_p} + \frac{1}{4}C_{n_r}C_{l_\beta}C_{Y_p}$$

$$E = \frac{1}{2}C_L\left(C_{n_r}C_{l_\beta} - C_{l_r}C_{n_\beta}\right) + \frac{1}{2}C_L \tan\gamma\left(C_{l_p}C_{n_\beta} - C_{n_p}C_{l_\beta}\right)$$

REFERENCES

1. Lichtenstein, Jacob H., and Williams, James L.: Effect of Frequency of Sideslipping Motion on the Lateral Stability Derivatives of a Typical Delta-Wing Airplane. NACA RM L57F07, 1957.

2. Queijo, M. J., Fletcher, Herman S., Marple, C. G., and Hughes, F. M.: Preliminary Measurements of the Aerodynamic Yawing Derivatives of a Triangular, a Swept, and an Unswept Wing Performing Pure Yawing Oscillations, With a Description of the Instrumentation Employed. NACA RM L55L14, 1956.

3. Fisher, Lewis R.: Experimental Determination of the Effects of Frequency and Amplitude on the Lateral Stability Derivatives for a Delta, a Swept, and an Unswept Wing Oscillating in Yaw. NACA Rep. 1357, 1958. (Supersedes NACA RM L56A19.)

4. Fisher, Lewis R., Lichtenstein, Jacob H., and Williams, Katherine D.: A Preliminary Investigation of the Effects of Frequency and Amplitude on the Rolling Derivatives of an Unswept-Wing Model Oscillating in Roll. NACA TN 3554, 1956.

5. Campbell, John P., and McKinney, Marion O.: Summary of Methods for Calculating Dynamic Lateral Stability and Response and for Estimating Lateral Stability Derivatives. NACA Rep. 1098, 1952. (Supersedes NACA TN 2409.)

6. MacLachlan, Robert, and Letko, William: Correlation of Two Experimental Methods of Determining the Rolling Characteristics of Unswept Wings. NACA TN 1309, 1947.

7. Goodman, Alex, and Thomas, David F., Jr.: Effects of Wing Position and Fuselage Size on the Low-Speed Static and Rolling Stability Characteristics of a Delta-Wing Model. NACA Rep. 1224, 1955. (Supersedes NACA TN 3063.)

8. Jaquet, Byron M., and Fletcher, Herman S.: Experimental Steady-State Yawing Derivatives of a 60° Delta-Wing Model As Affected by Changes in Vertical Position of the Wing and in Ratio of Fuselage Diameter to Wing Span. NACA TN 3843, 1956.

9. Sternfield, Leonard, and Gates, Ordway B., Jr.: A Simplified Method for the Determination and Analysis of the Neutral-Lateral-Oscillatory-Stability Boundary. NACA Rep. 943, 1949. (Supersedes NACA TN 1727.)

TABLE I.- GEOMETRIC PROPERTIES OF MODEL

Fuselage:	
Length, in.	54.0
Maximum diameter, in.	6.0
Fineness ratio	9.0
Body-size ratio, d/b	0.164
Volume, cu in.	990
Side area, sq in.	252
Wing:	
Aspect ratio	2.31
Taper ratio	0
Leading-edge sweep angle, deg	60
Airfoil section	NACA 65A003
Area, sq in.	576.7
Span, in.	36.5
Mean aerodynamic chord, in.	21.1
Root chord, in.	31.6
Vertical tail:	
Aspect ratio	2.18
Taper ratio	0
Leading-edge sweep angle, deg	42.5
Airfoil section	NACA 65-006
Area, sq in.	66.0
Span, in.	12.00
Root chord, in.	11.00
Mean aerodynamic chord, in.	7.35
Tail length, in.	21.5

TABLE II.- CALCULATION CONDITIONS FOR AIRPLANE PERIOD AND DAMPING

$\left[\mu = 11.85;\ \gamma = 0^{\circ};\ h = 0;\ \text{and}\ \ b = 39.1\ \text{ft}\right]$

Flight conditions				Mass parameters			Aerodynamic derivatives										
α	η	C_L	V	K_X^2	K_Z^2	K_{XZ}	C_{l_p}	C_{n_p}	C_{Y_p}	C_{l_r}	C_{n_r}	C_{Y_r}	C_{l_β}	C_{n_β}	C_{Y_β}	$C_{l_{\dot{p},\omega}}$	$C_{n_{\dot{p},\omega}}$
2	0.8	0.059	701	0.0135	0.0841	-0.0010	-0.160	0.015	0.060	0.075	-0.300	0.390	-0.085	0.180	-0.478	0.022	0.356
10	8.8	.349	289	.0151	.0829	-.0107	-.160	-.030	.170	.056	-.300	.400	-.140	.195	-.520	.090	.412
16	14.8	.581	223	.0181	.0798	-.0175	-.175	-.070	.300	.025	-.300	.420	-.120	.194	-.535	.004	.464
20	18.8	.720	201	.0210	.0767	-.0216	-.195	-.095	.390	-.015	-.300	.400	-.100	.180	-.520	.029	.517
22	20.8	.780	193	.0224	.0755	-.0235	-.225	-.100	.435	-.040	-.290	.395	-.082	.142	-.475	.034	.550
24	22.8	.830	187	.0242	.0737	-.0253	-.260	-.095	.435	-.083	-.255	.392	-.055	.068	-.376	.021	.640

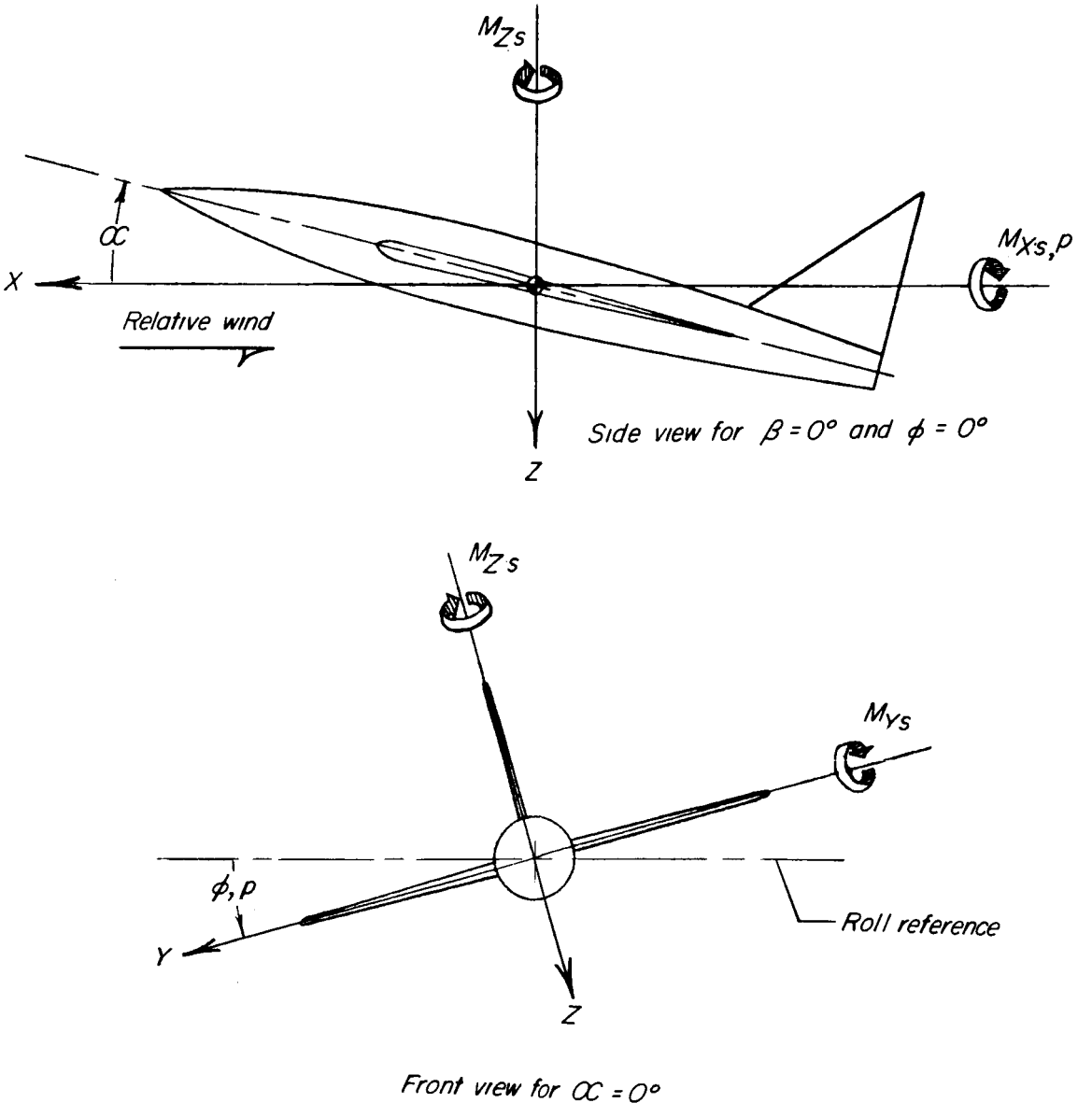

Figure 1.- System of stability axes. Arrows indicate positive forces, moments, angular displacements, and angular velocities.

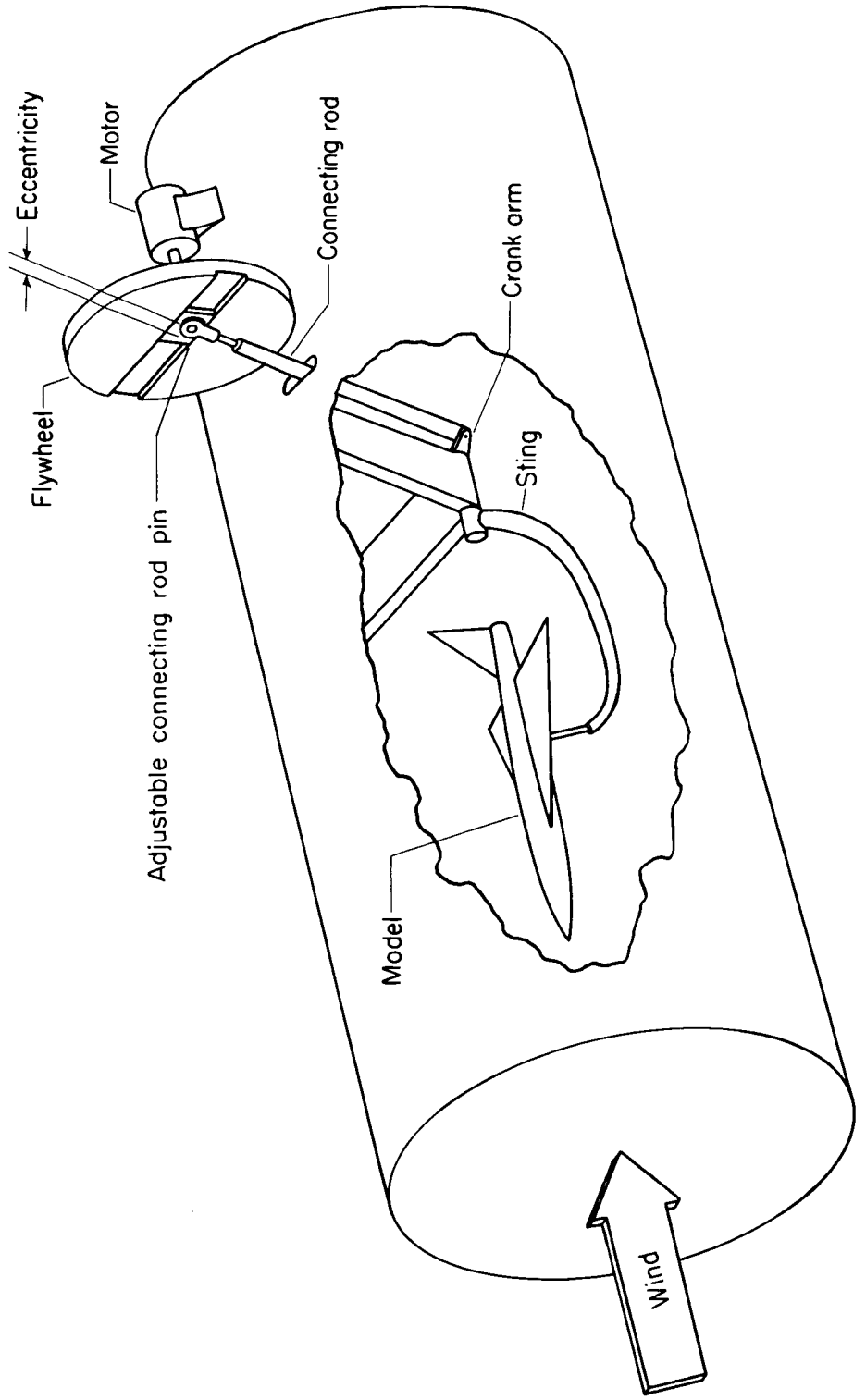

Figure 2.- Schematic diagram of test section and oscillation equipment.

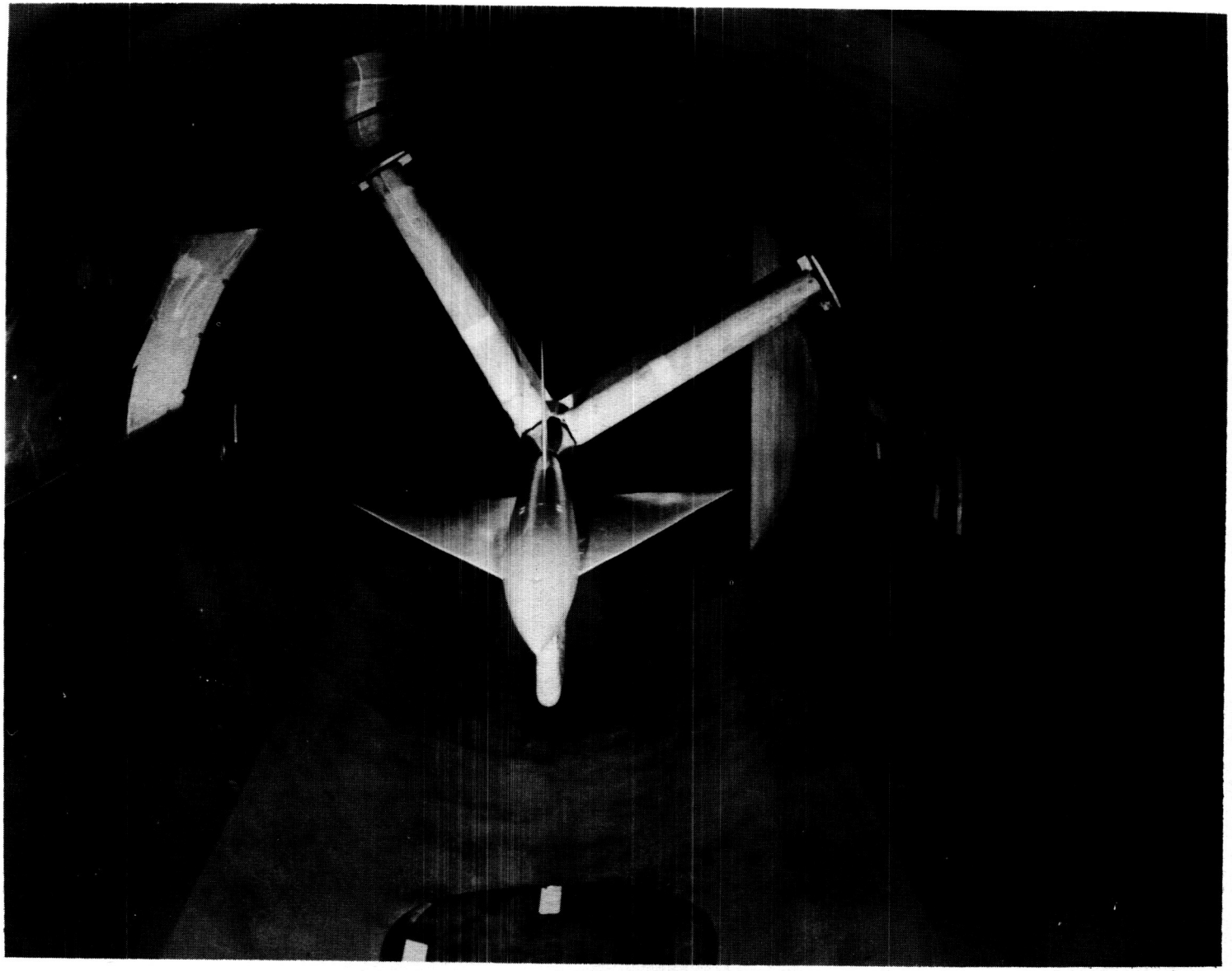

L-94432.1

Figure 3.- Photograph of model and model support in test section.

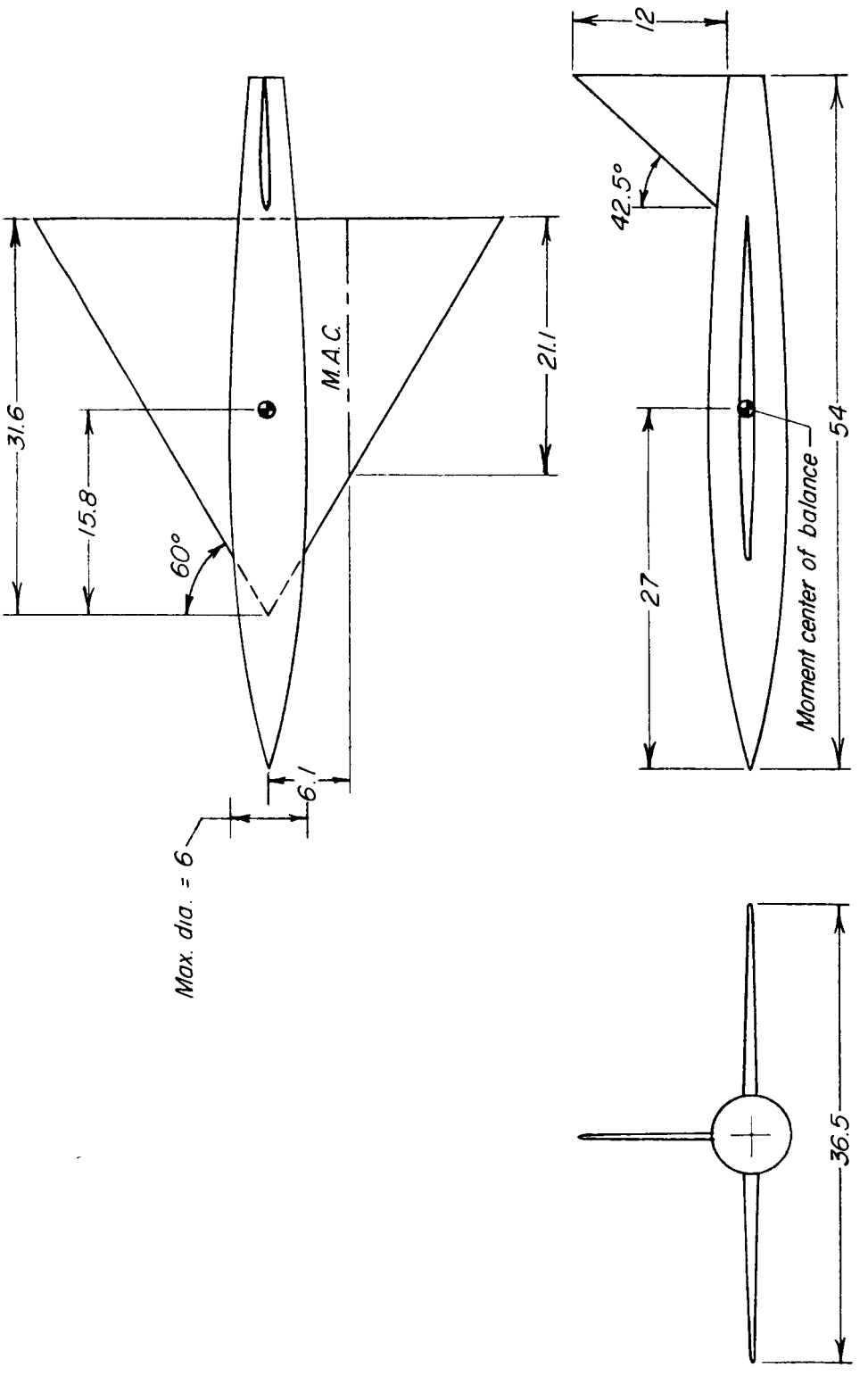

Figure 4.- Drawing of model tested. All dimensions are in inches.

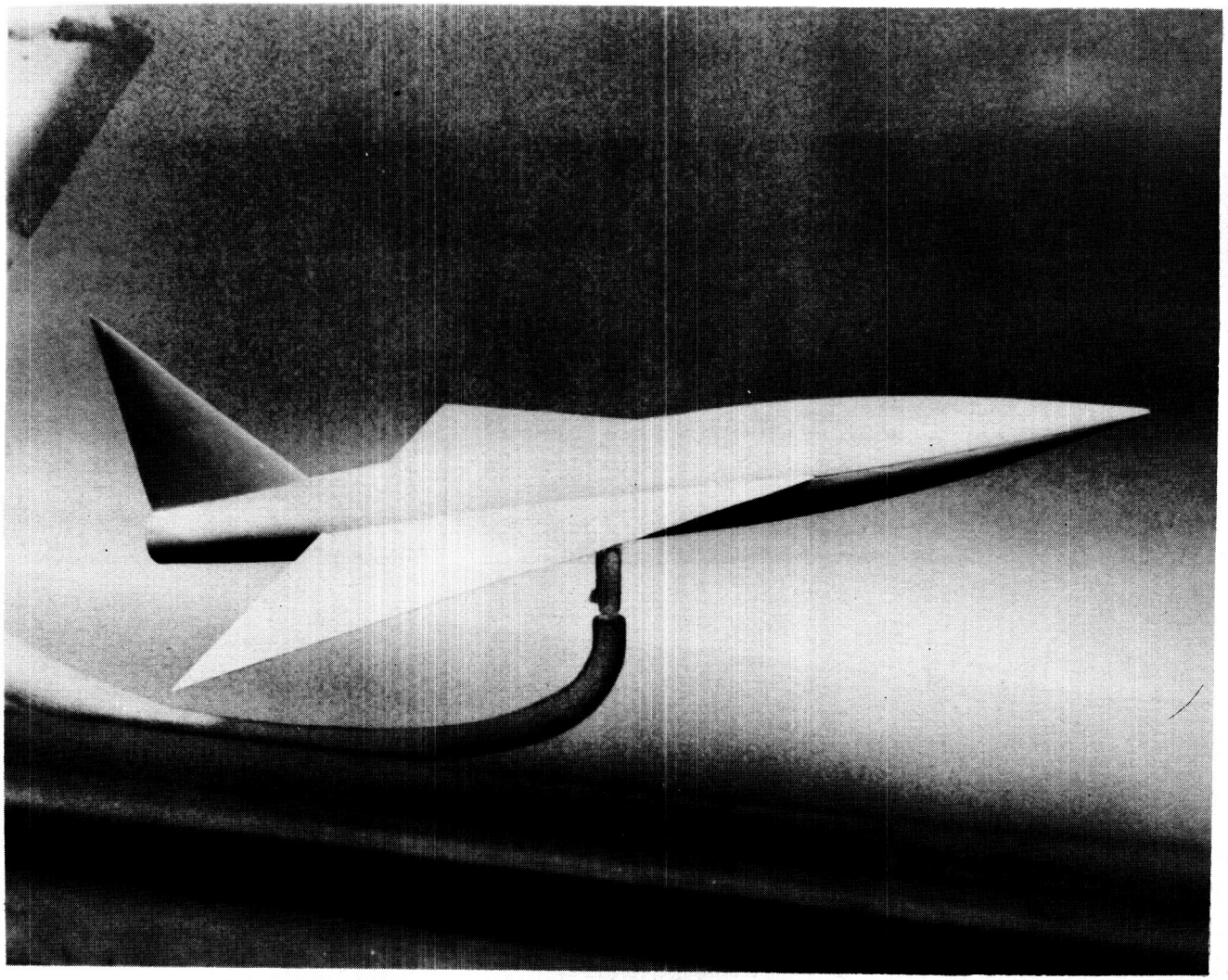

L-94431.1

Figure 5.- Photograph of complete model mounted on oscillation sting support.

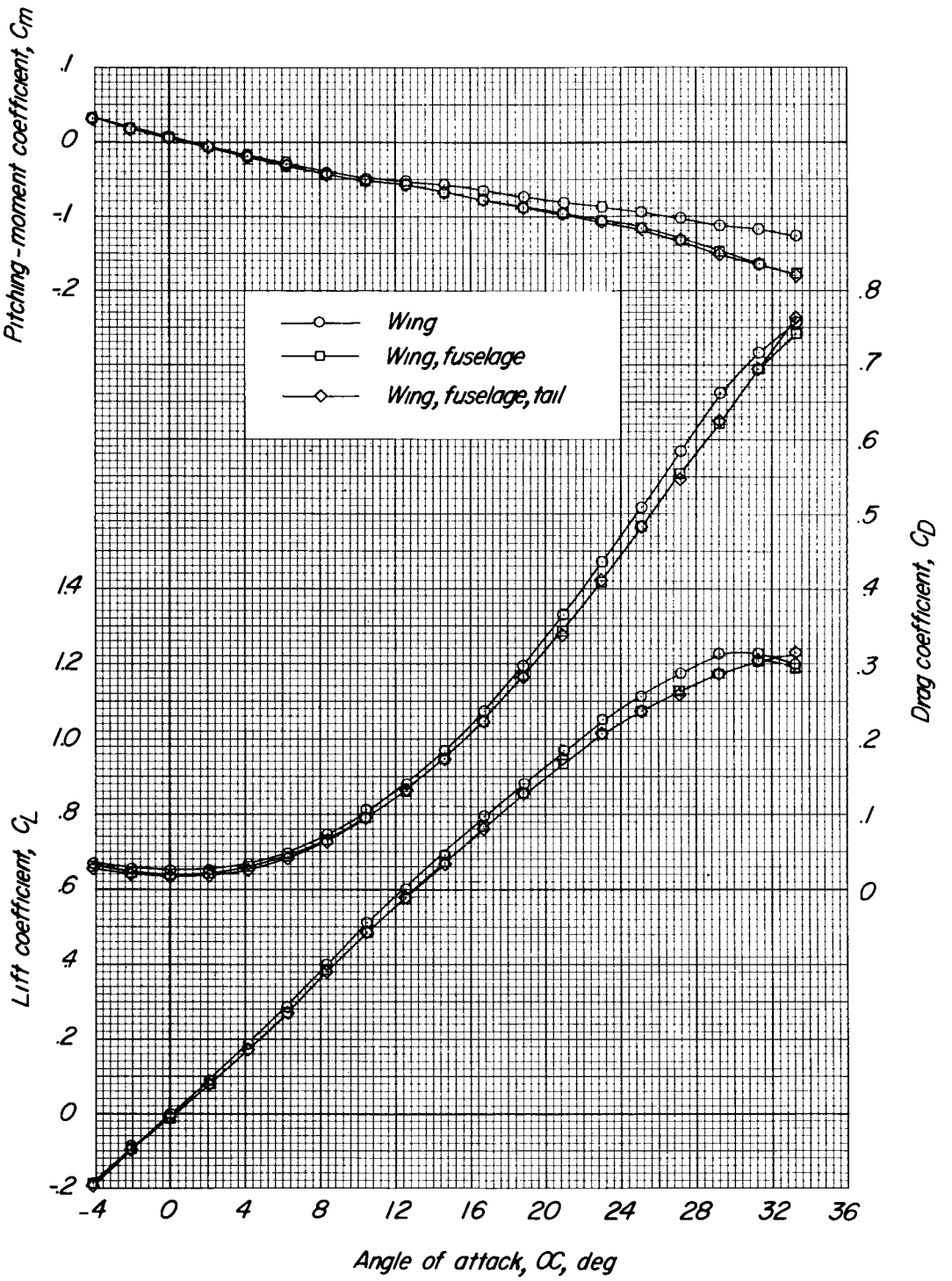

Figure 6.- Lift, drag, and pitching-moment curves for the model tested.

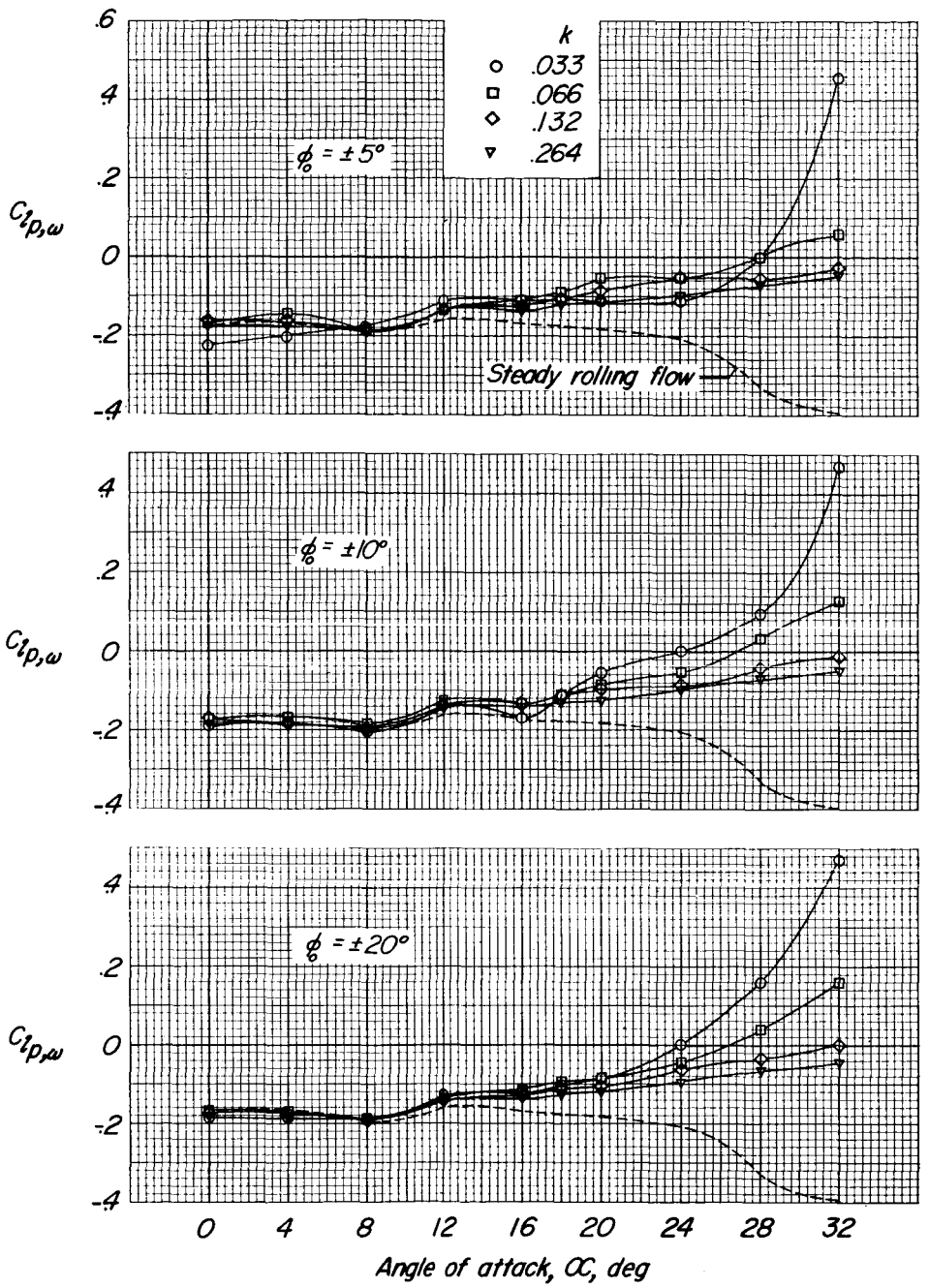

(a) Wing alone.

Figure 7.- The effects of amplitude and frequency of oscillation on the damping in roll.

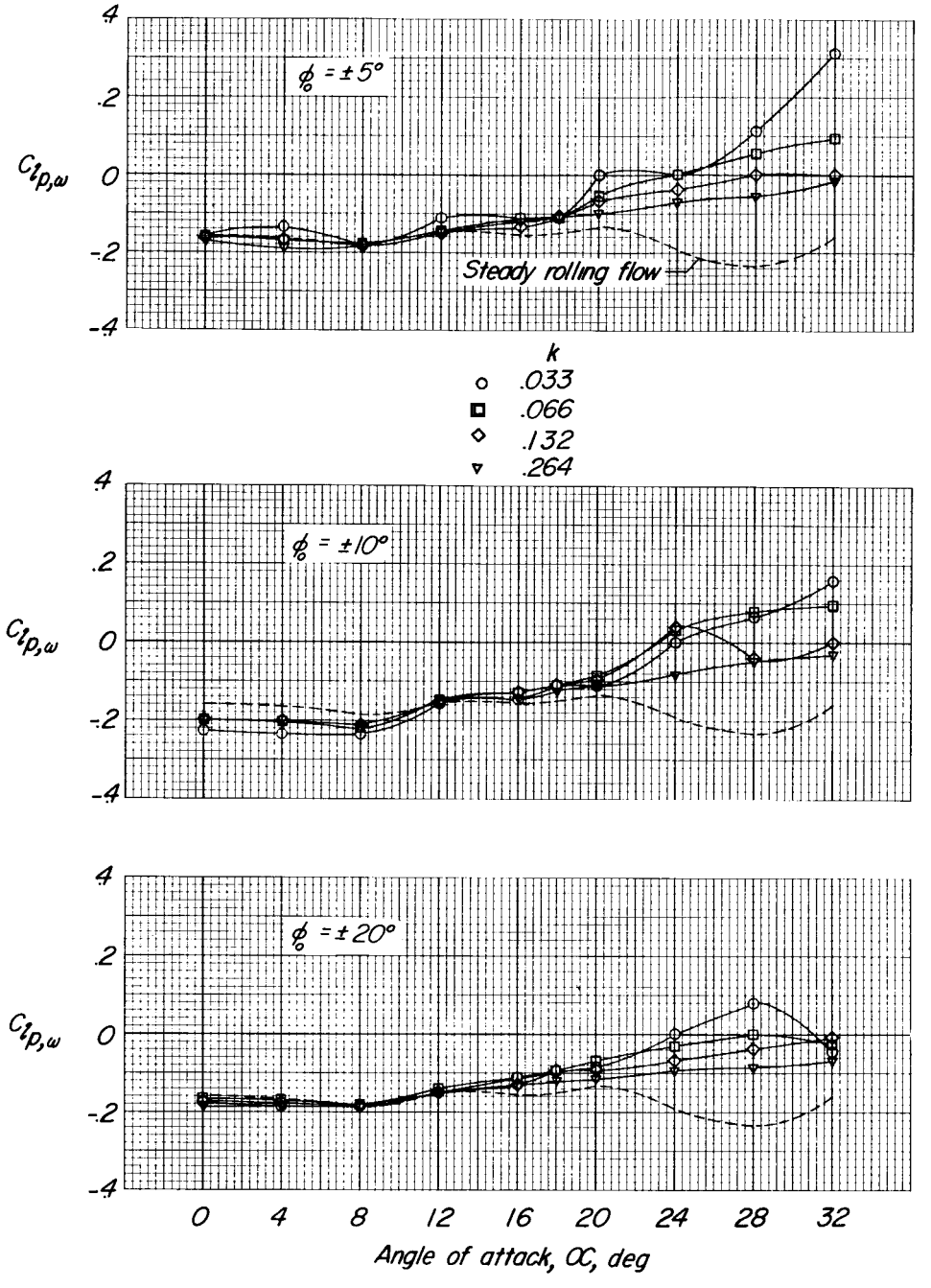

(b) Wing and fuselage.

Figure 7.- Continued.

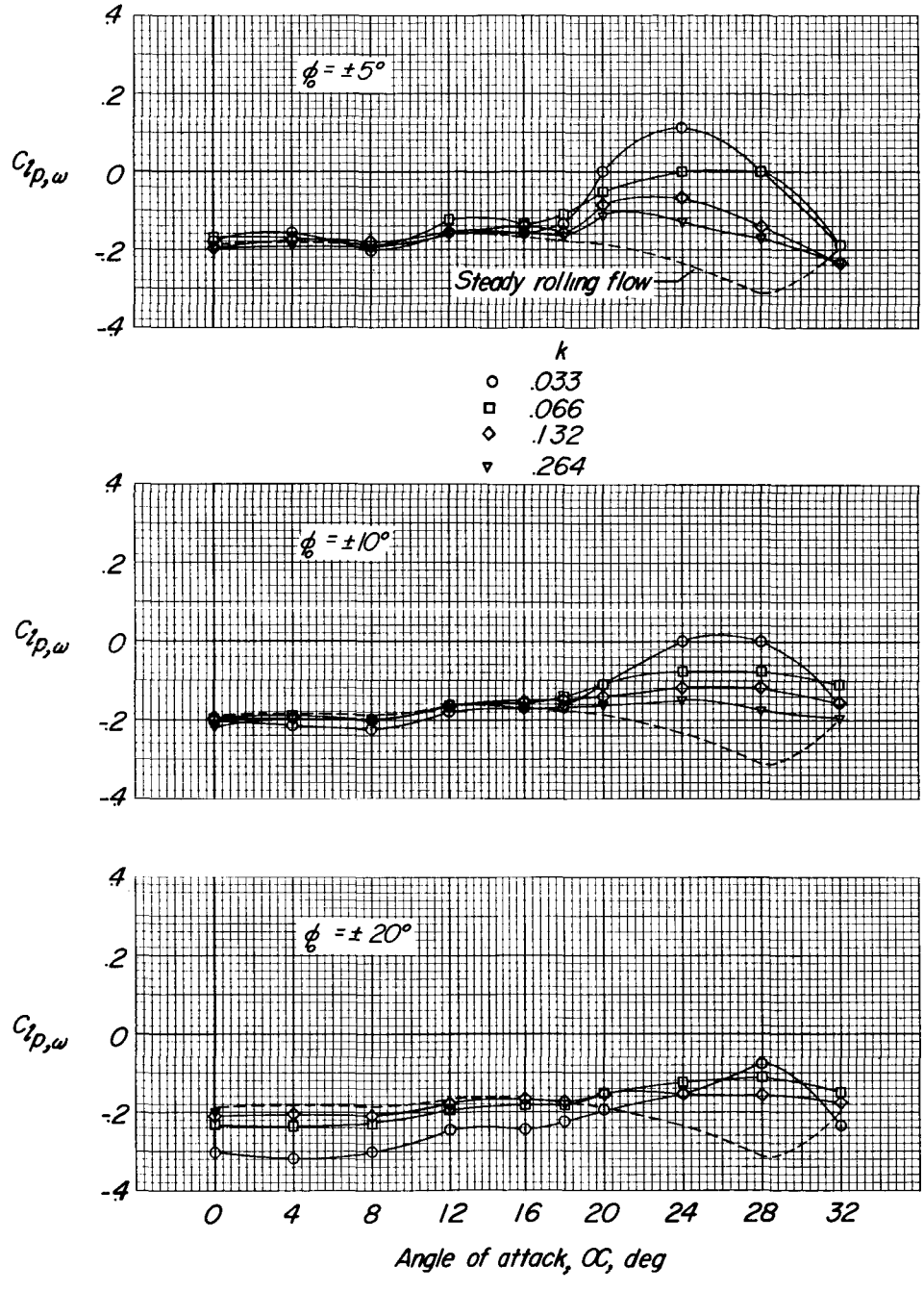

(c) Wing, fuselage, and tail.

Figure 7.- Concluded.

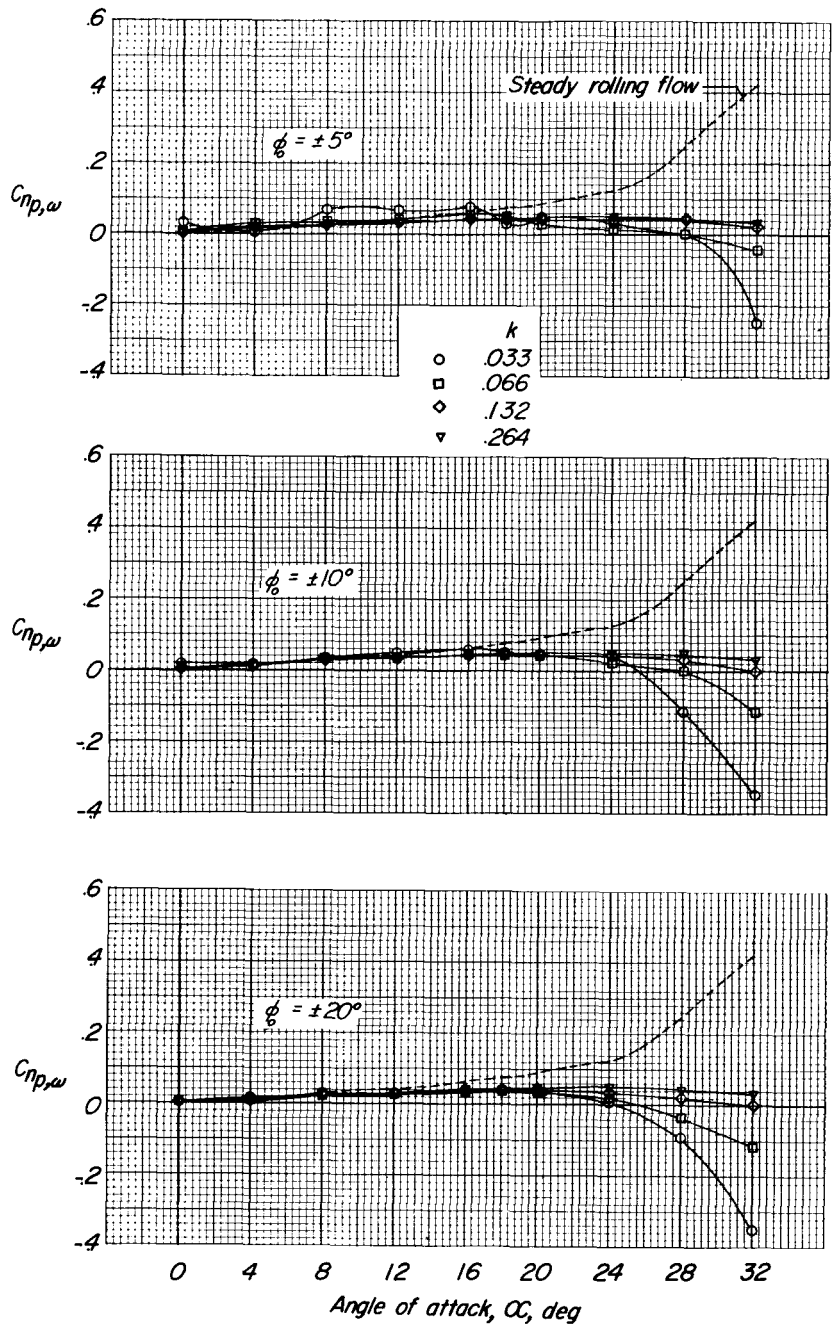

(a) Wing alone.

Figure 8.- The effects of amplitude and frequency of oscillation on the yawing moment due to rolling velocity.

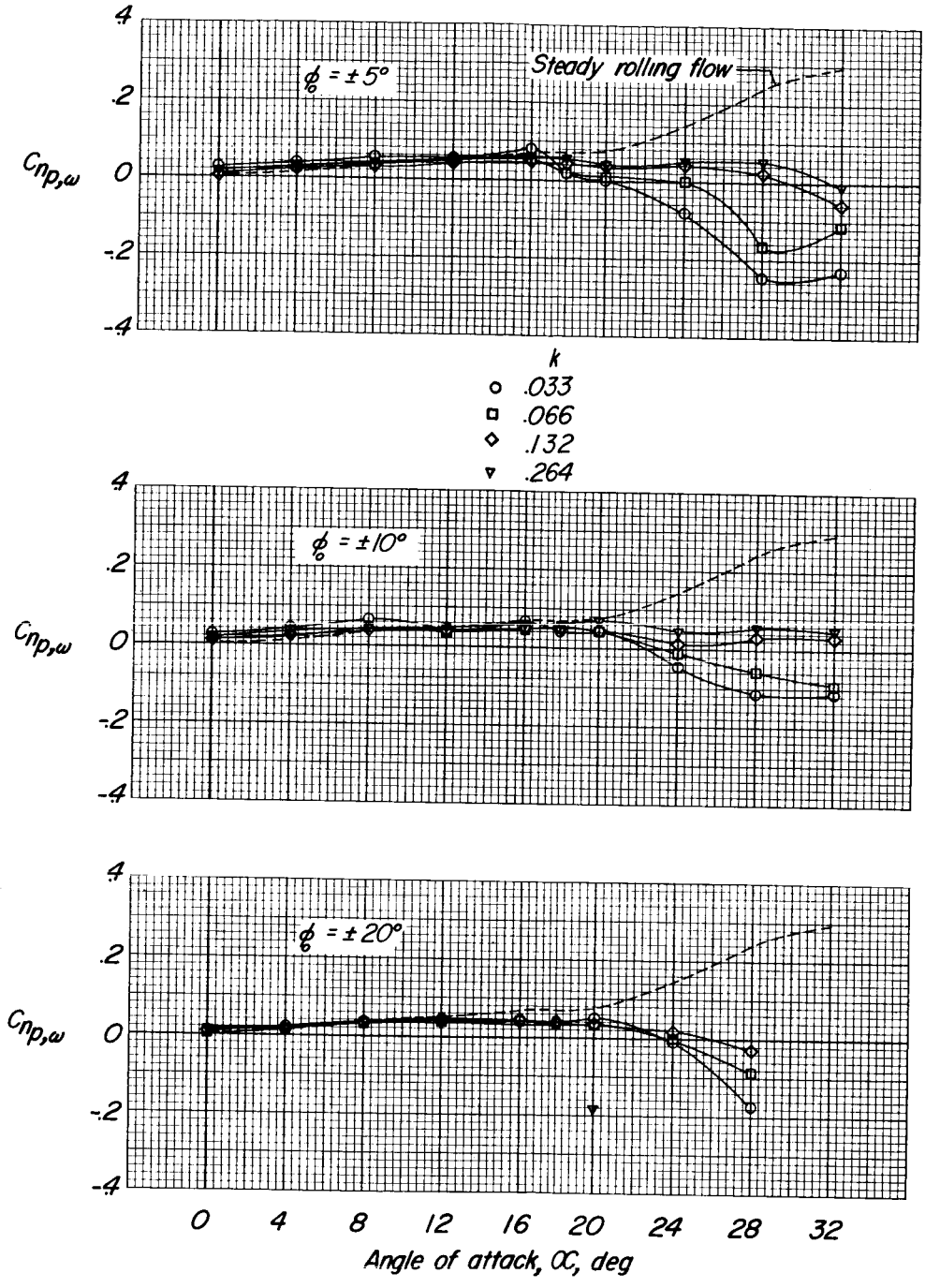

(b) Wing and fuselage.

Figure 8.- Continued.

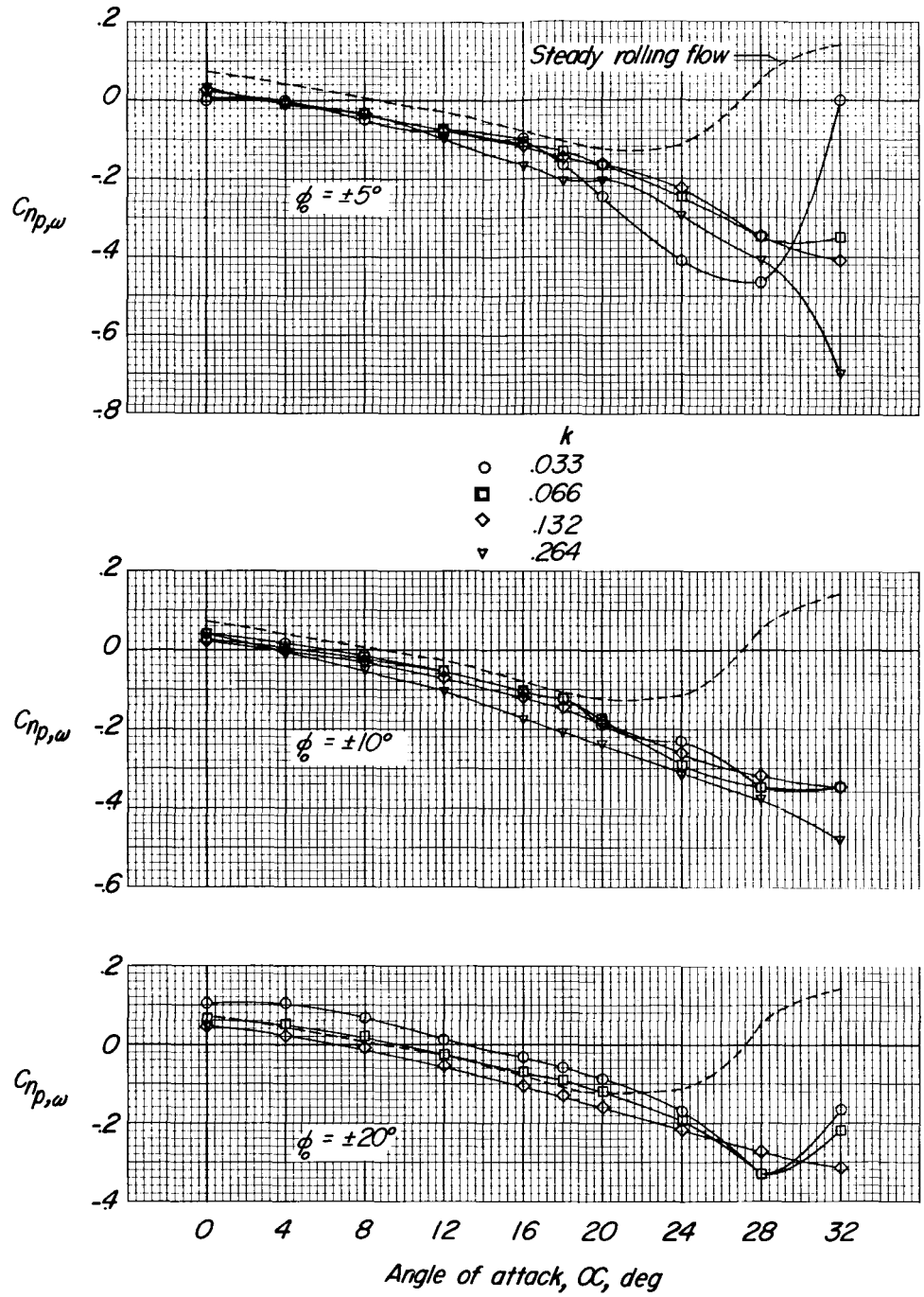

(c) Wing, fuselage, and tail.

Figure 8.- Concluded.

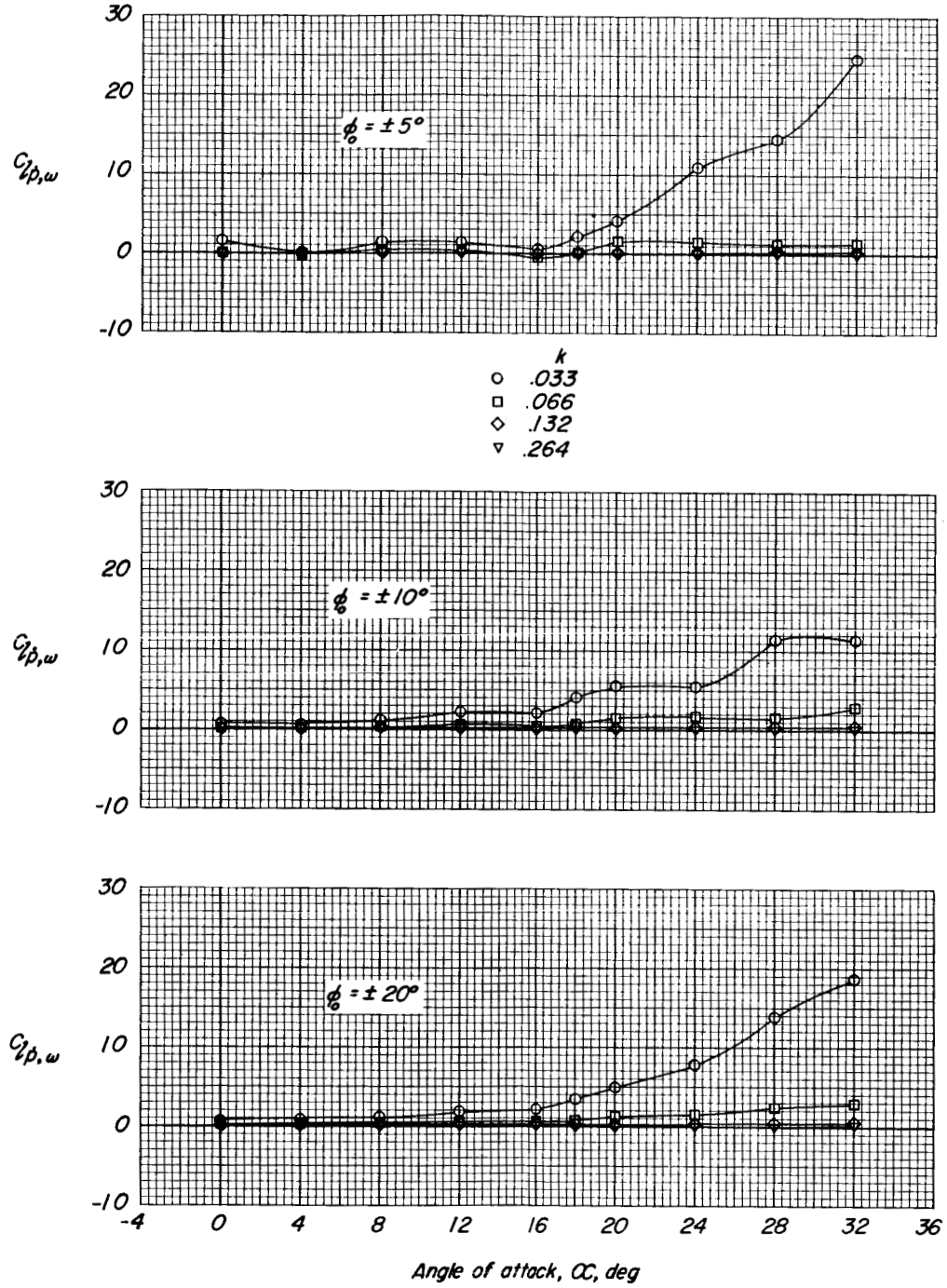

(a) Wing alone.

Figure 9.- The effects of amplitude and frequency of oscillation on the rolling moment due to rolling acceleration.

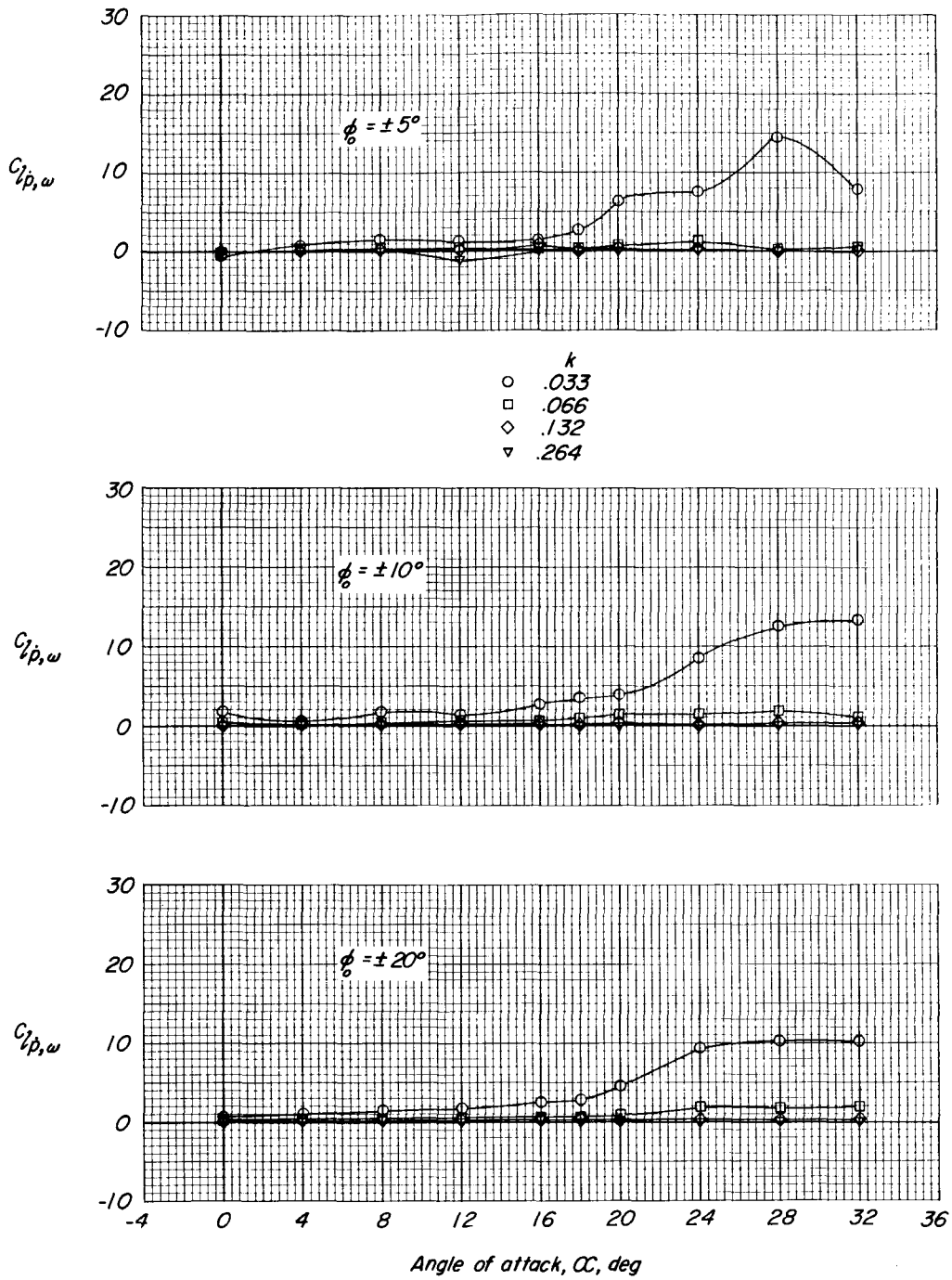

(b) Wing and fuselage.

Figure 9.- Continued.

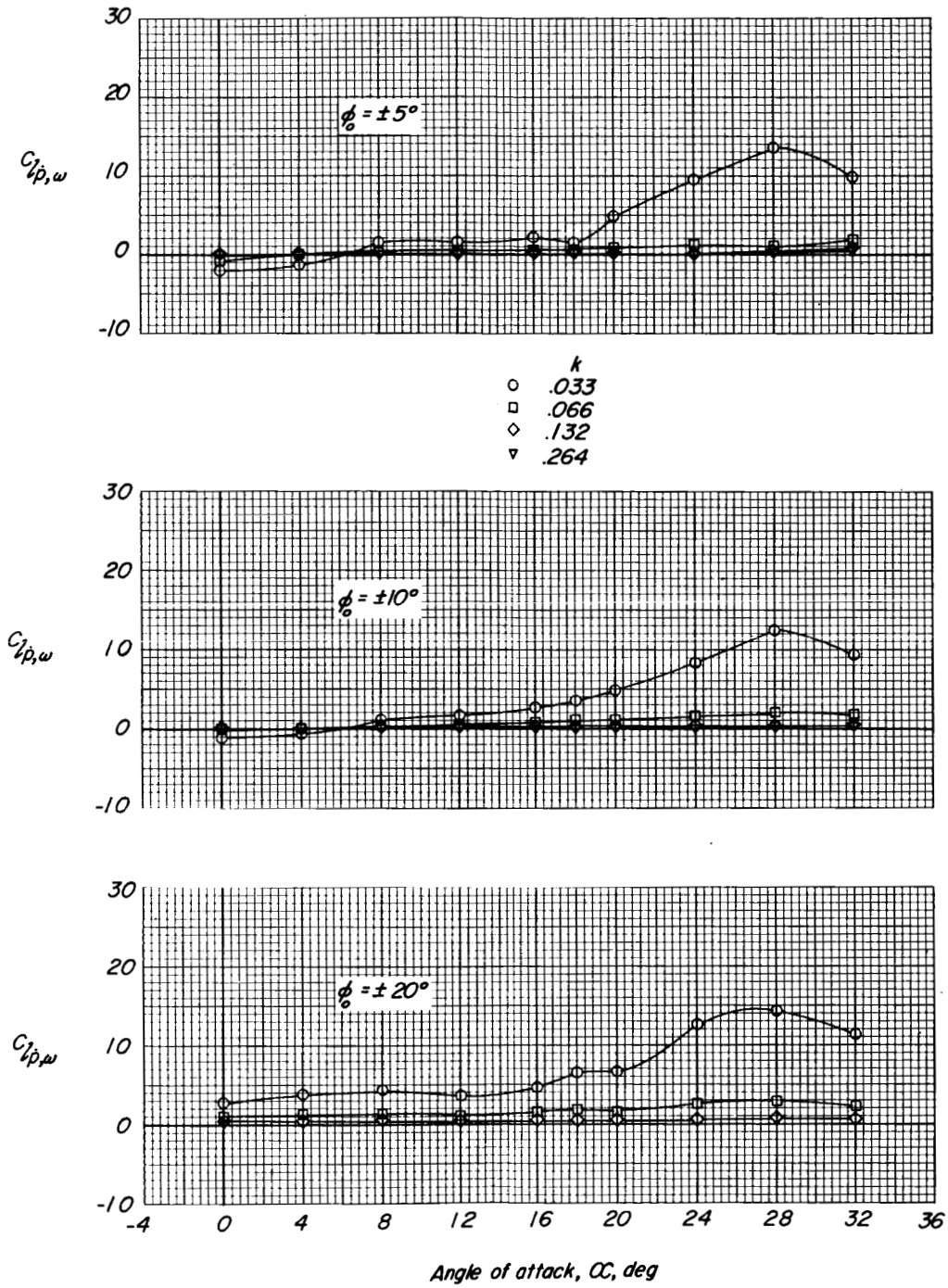

(c) Wing, fuselage, and tail.

Figure 9.- Concluded.

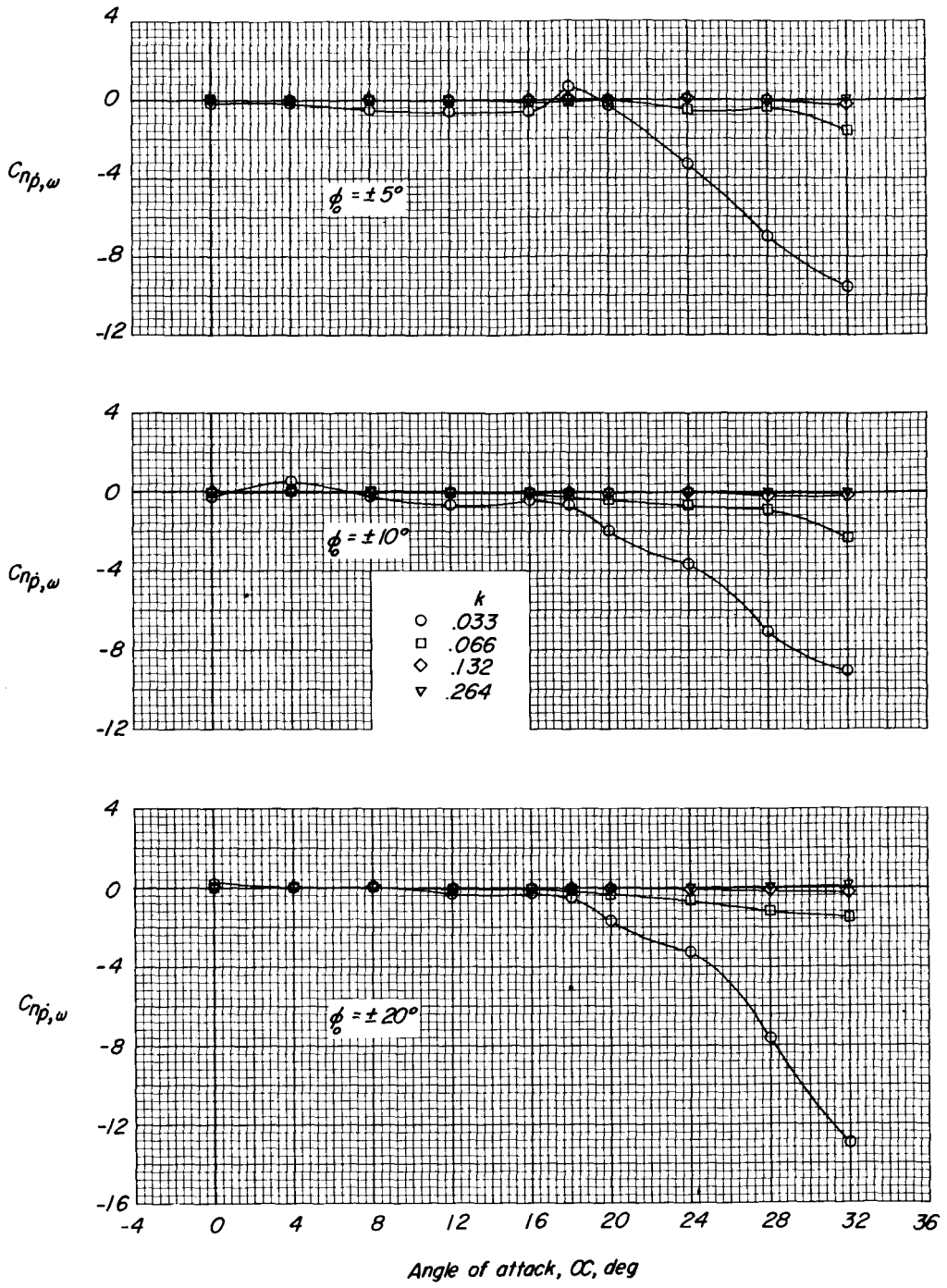

(a) Wing alone.

Figure 10.- The effects of amplitude and frequency of oscillation on the yawing moment due to rolling acceleration.

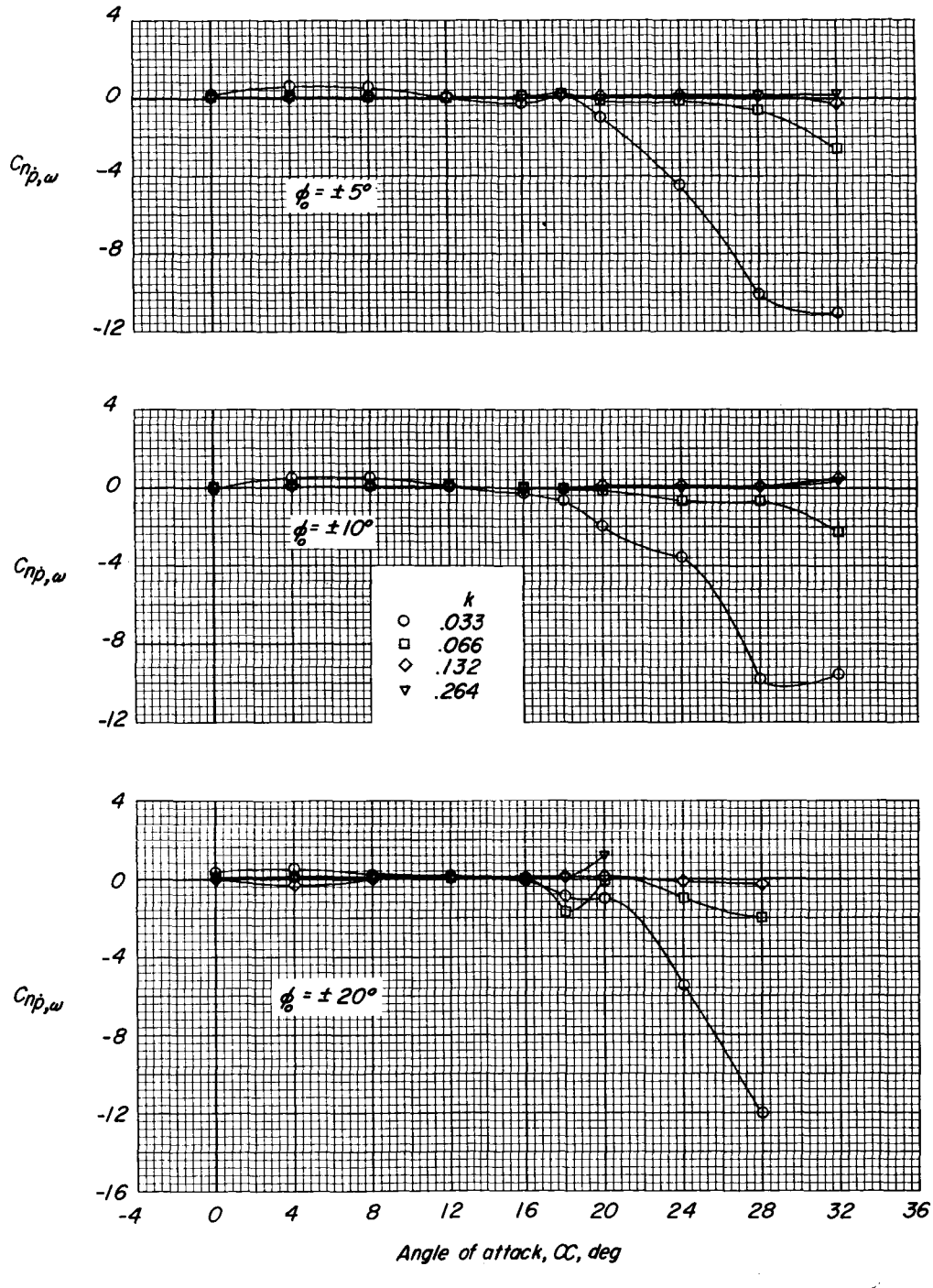

(b) Wing and fuselage.

Figure 10.- Continued.

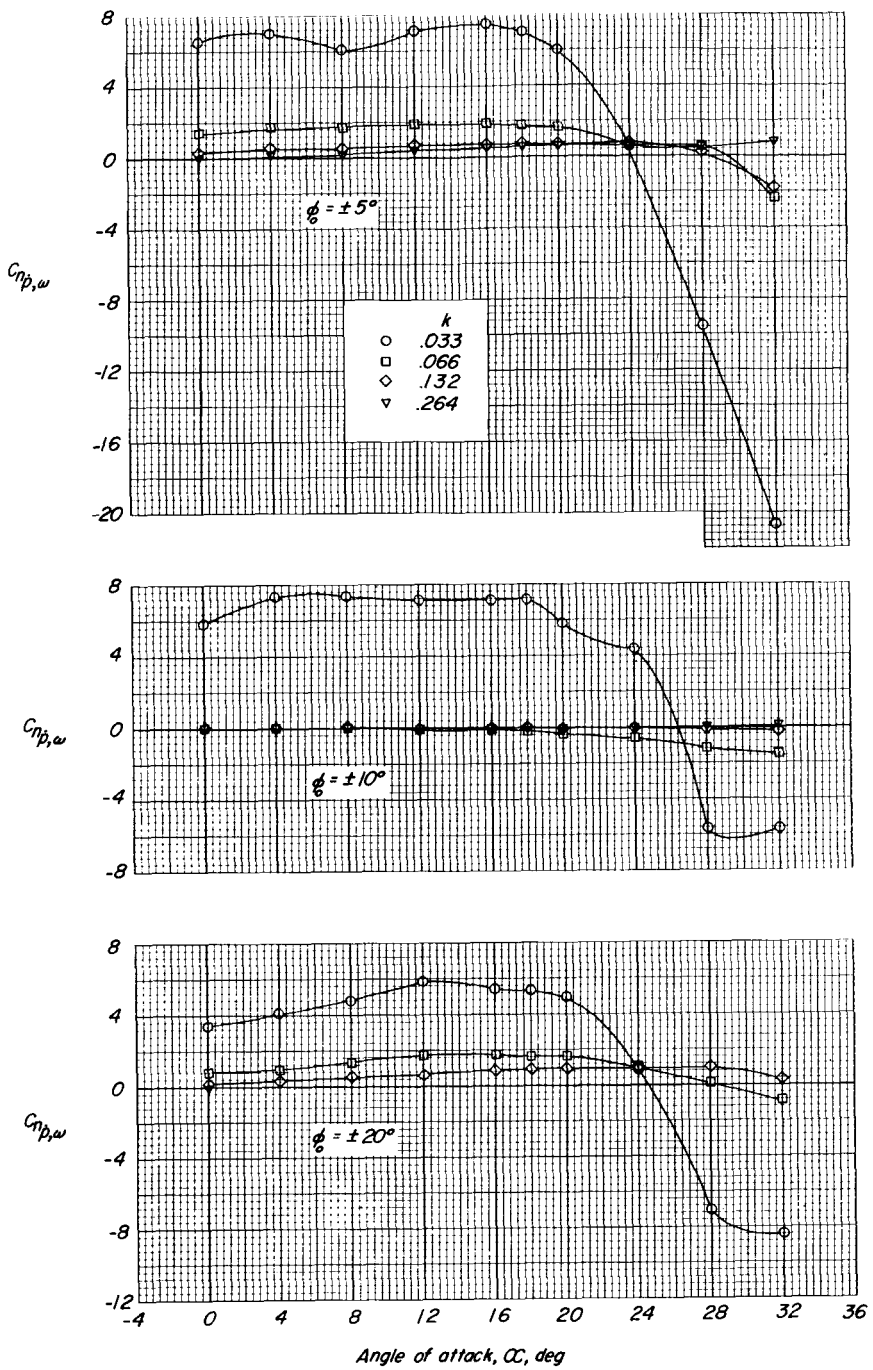

(c) Wing, fuselage, and tail.

Figure 10.- Concluded.

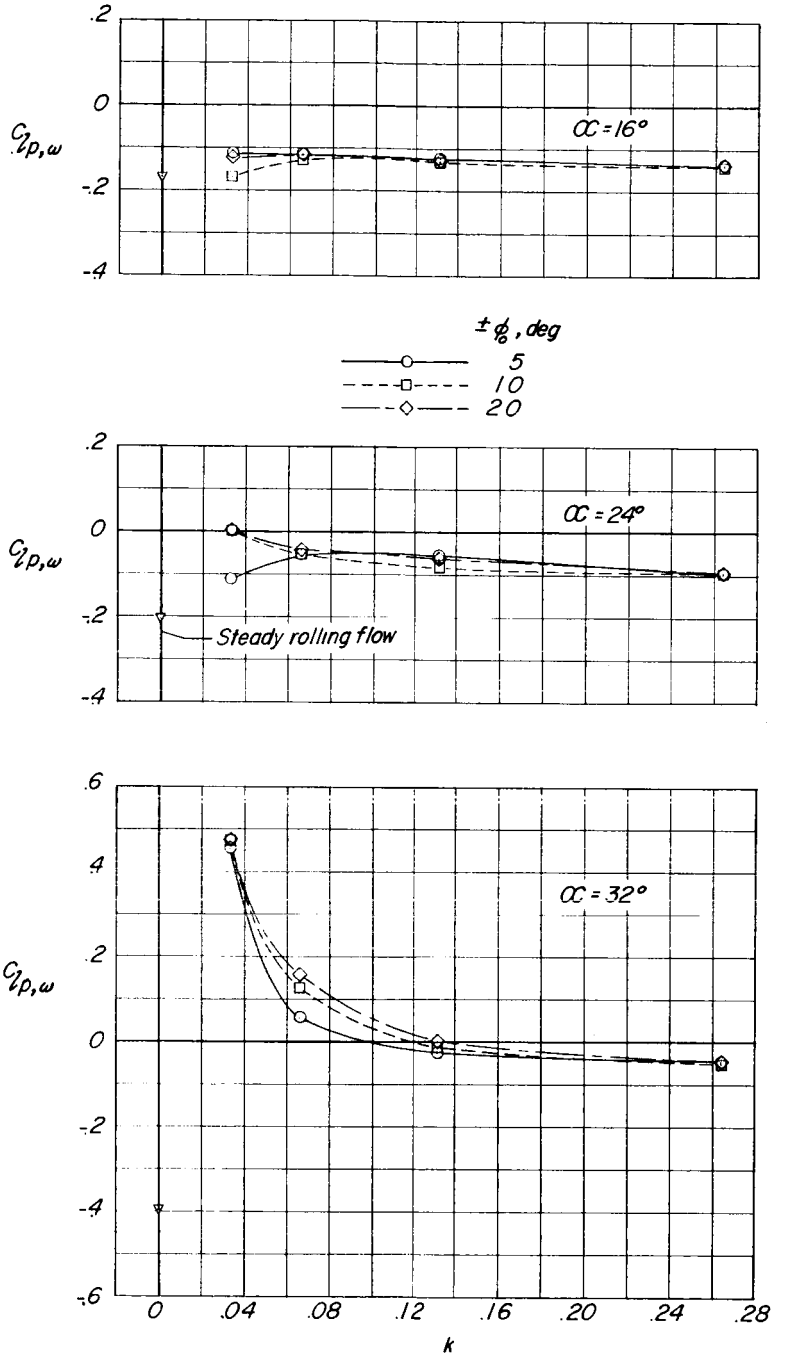

(a) Wing alone.

Figure 11.- The damping in roll as a function of reduced frequency of oscillation for three high angles of attack.

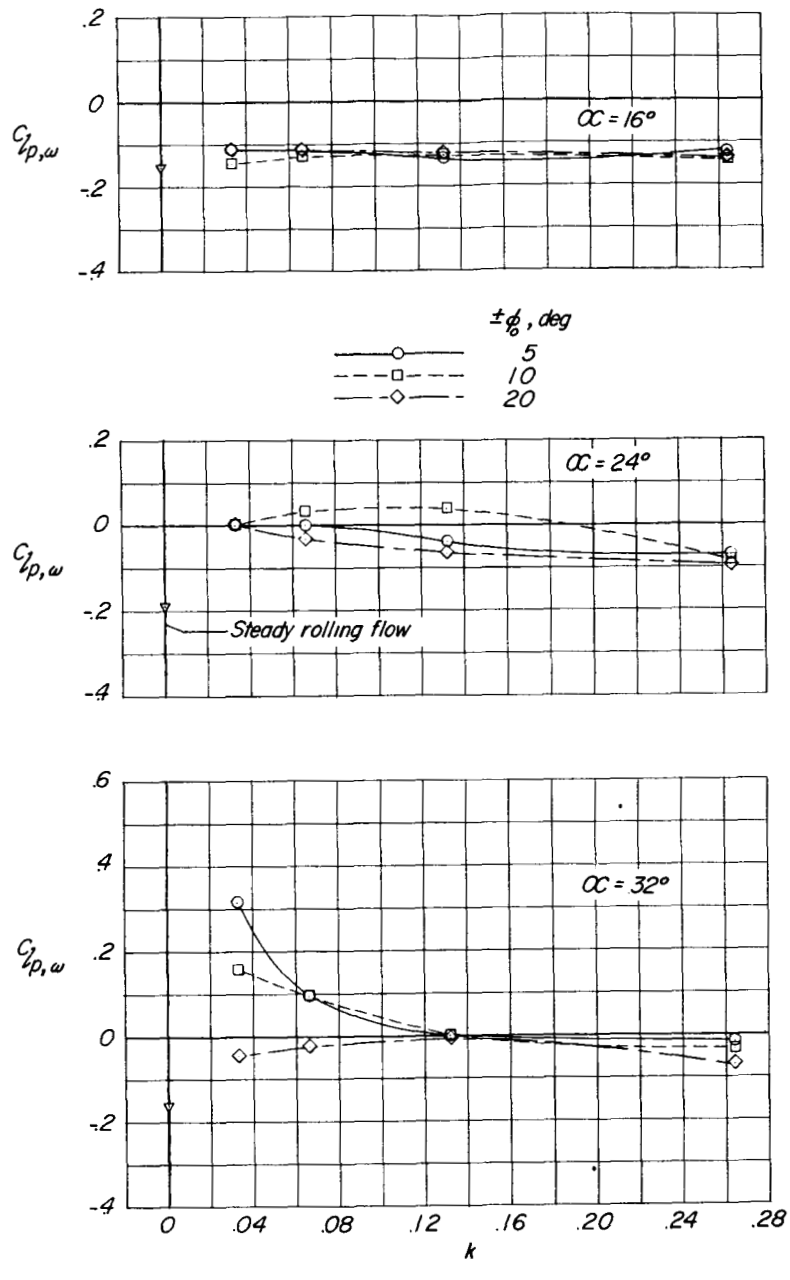

(b) Wing and fuselage.

Figure 11.- Continued.

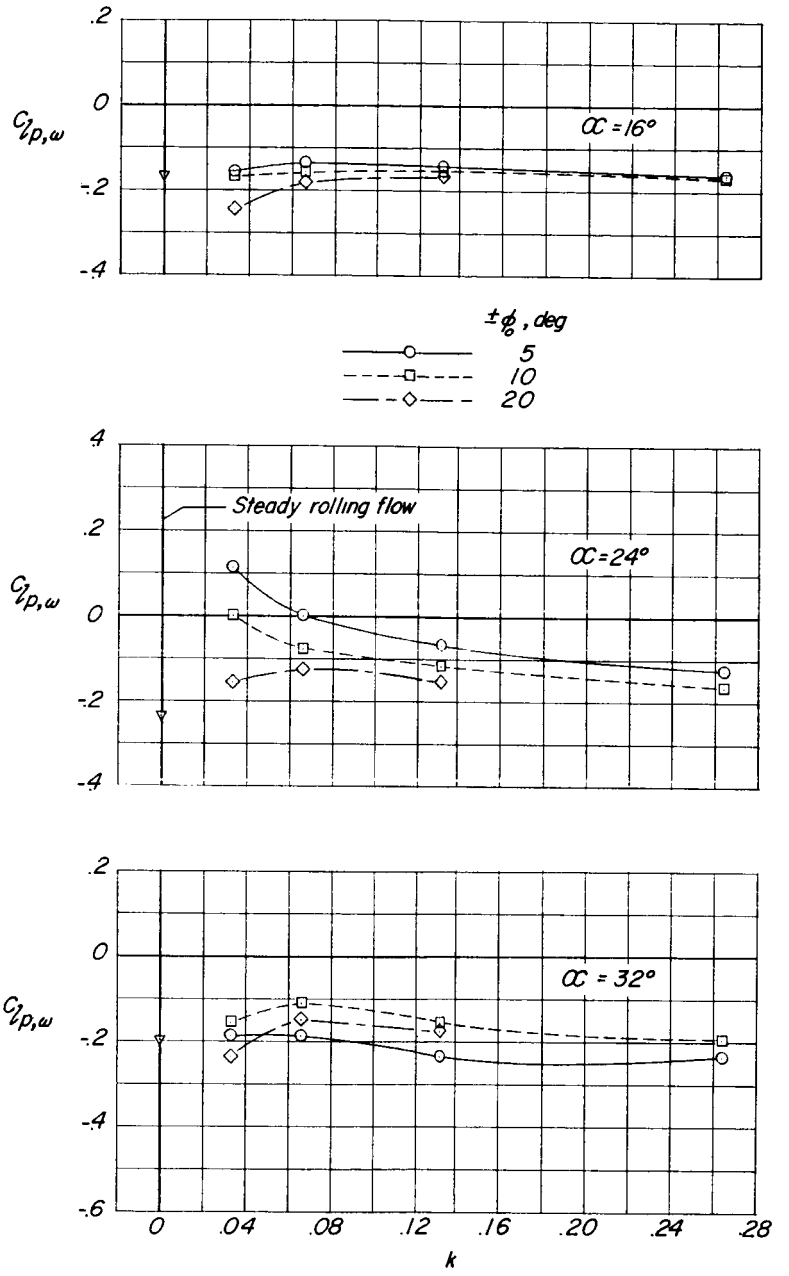

(c) Wing, fuselage, and tail.

Figure 11.- Concluded.

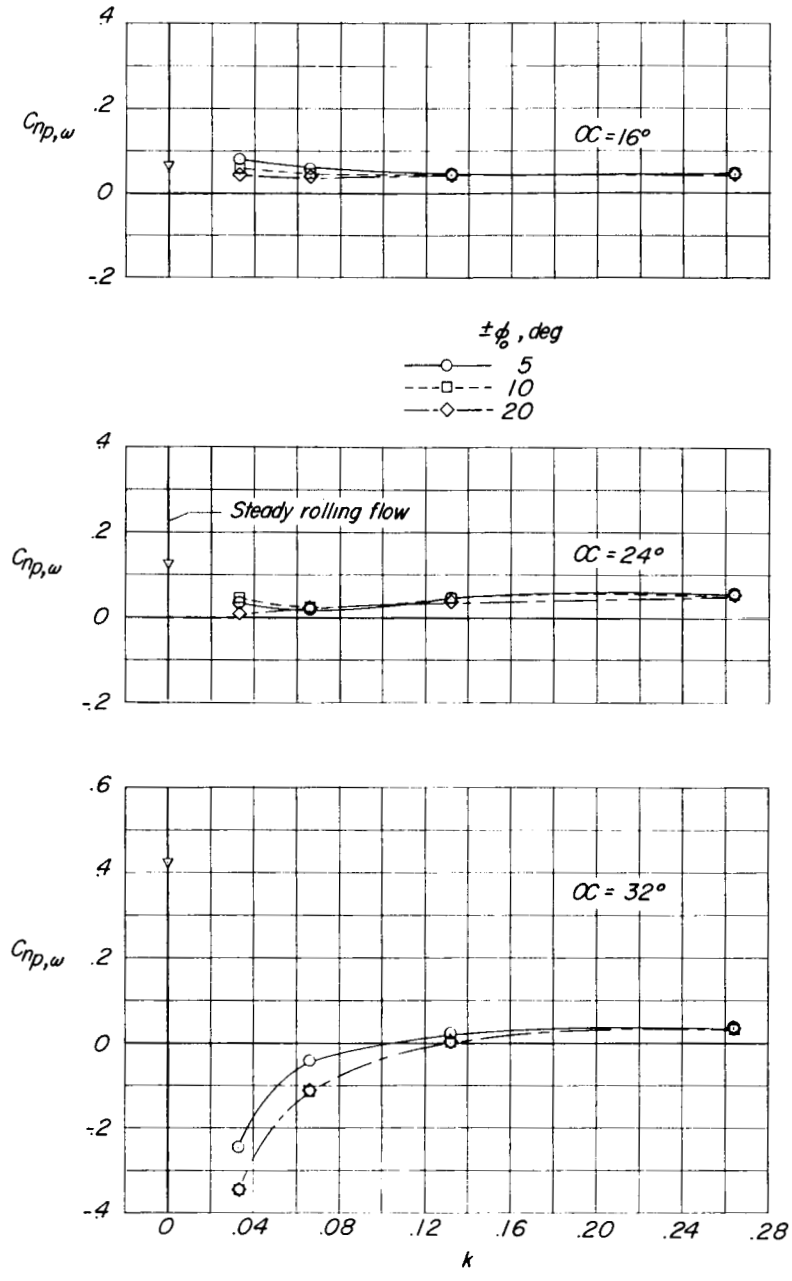

(a) Wing alone.

Figure 12.- The yawing moment due to rolling velocity as a function of reduced frequency of oscillation for three high angles of attack.

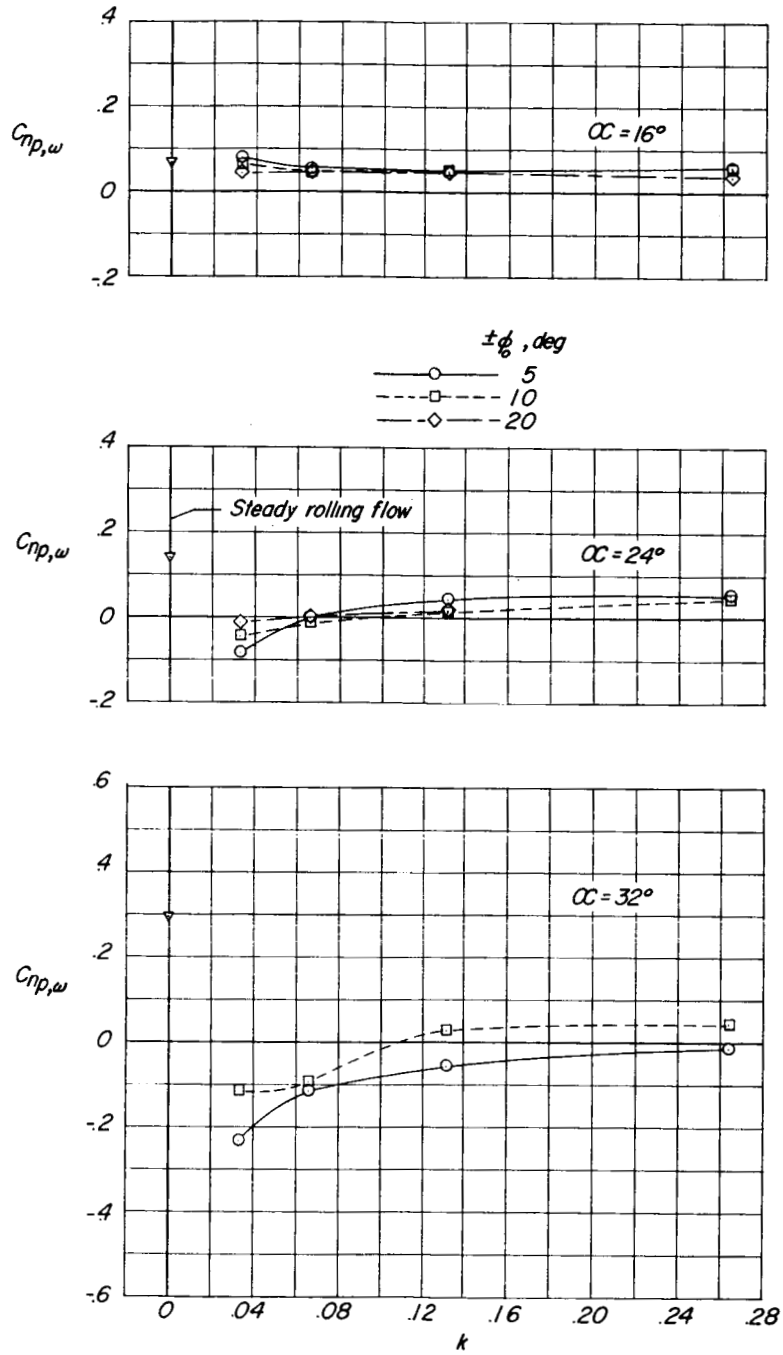

(b) Wing and fuselage.

Figure 12.- Continued.

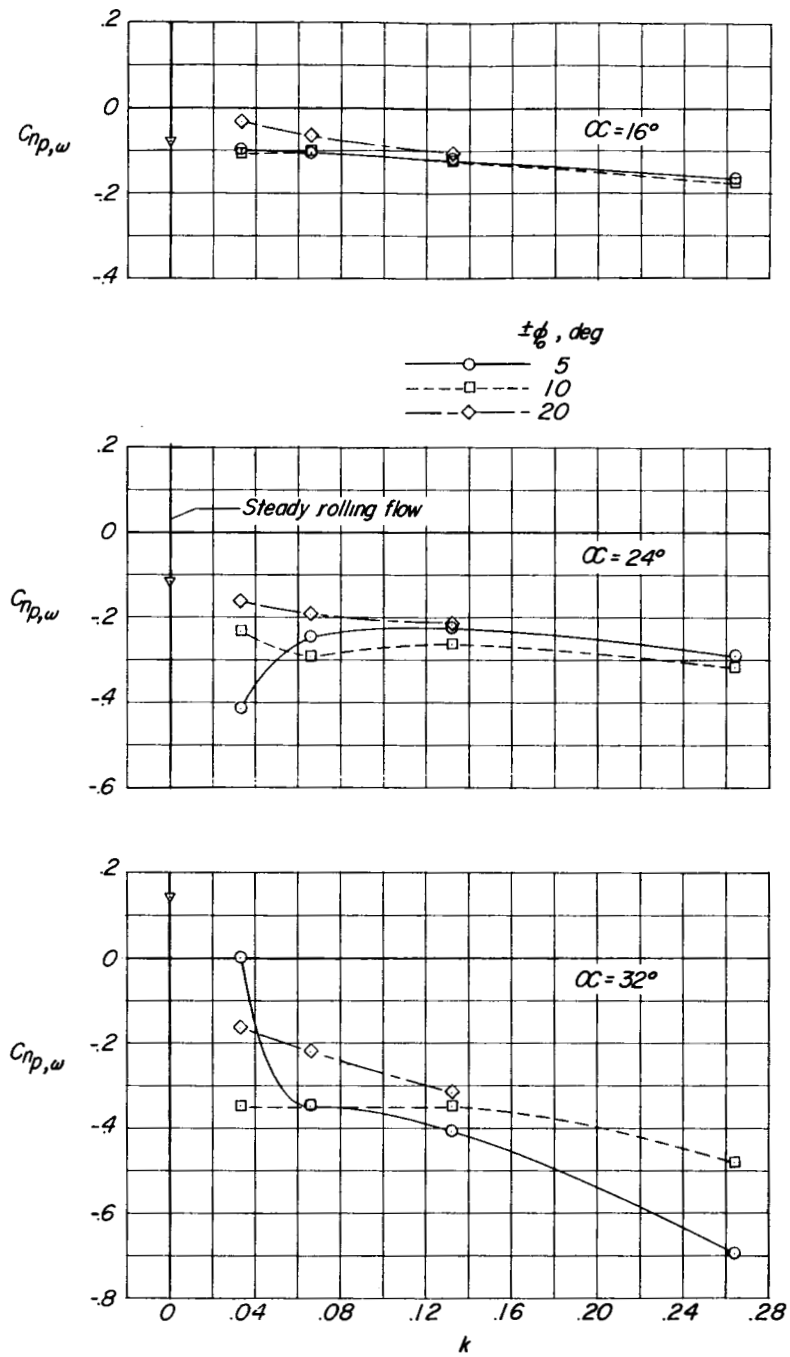

(c) Wing, fuselage, and tail.

Figure 12.- Concluded.

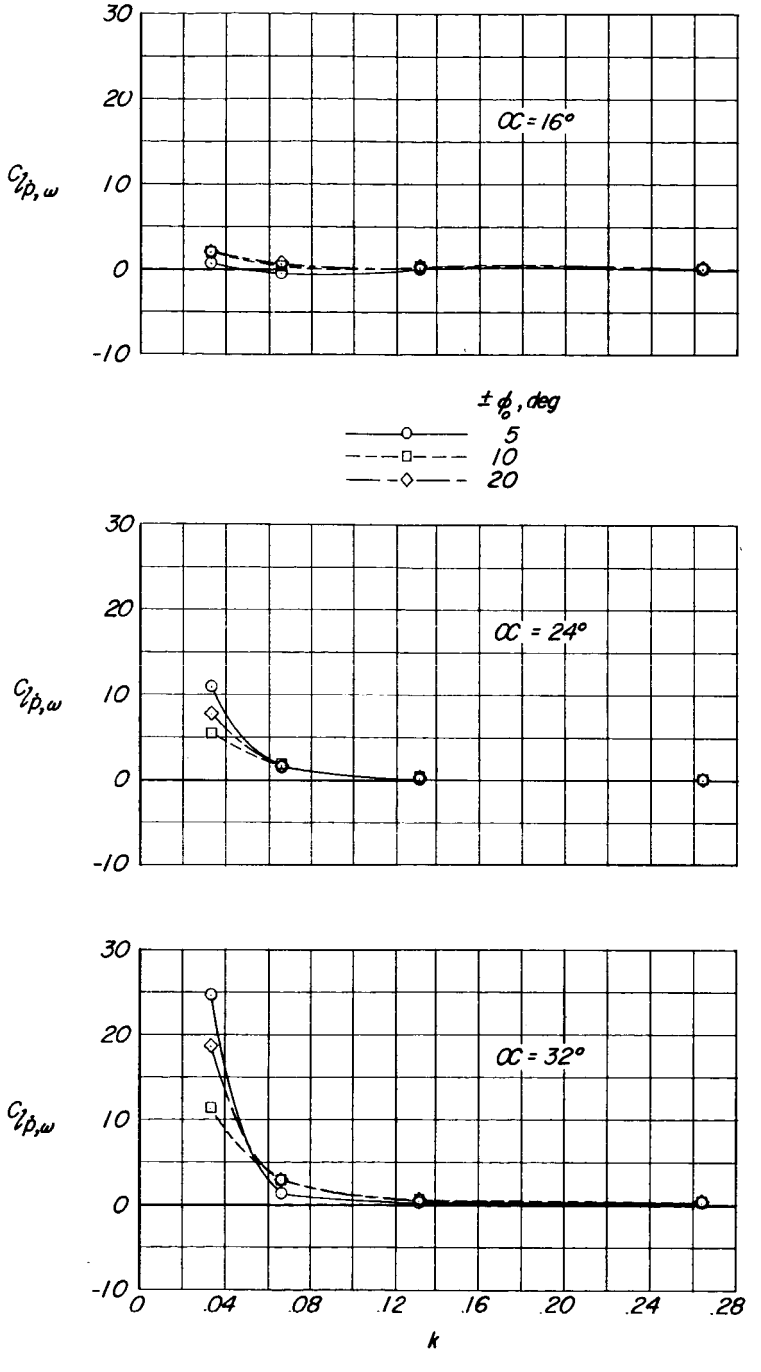

(a) Wing alone.

Figure 13.- The rolling moment due to rolling acceleration as a function of reduced frequency of oscillation for three high angles of attack.

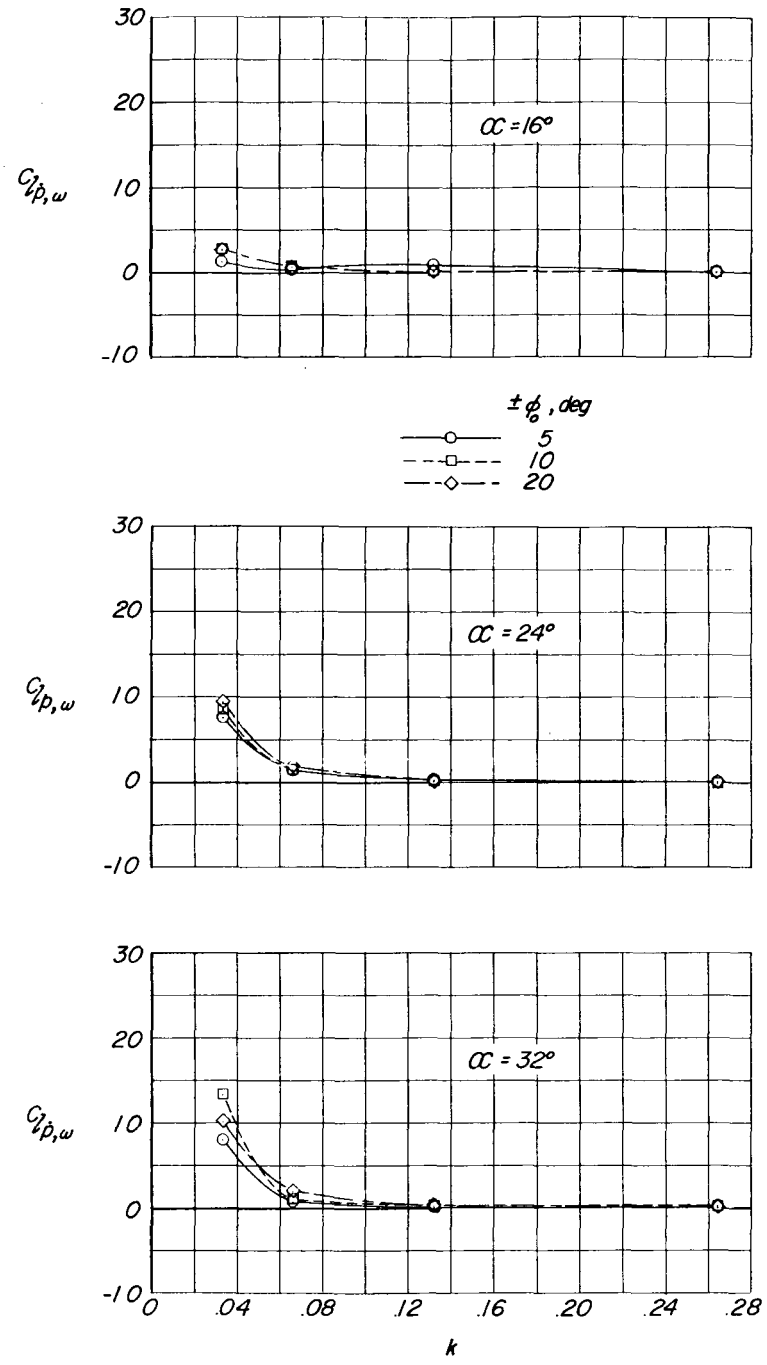

(b) Wing and fuselage.

Figure 13.- Continued.

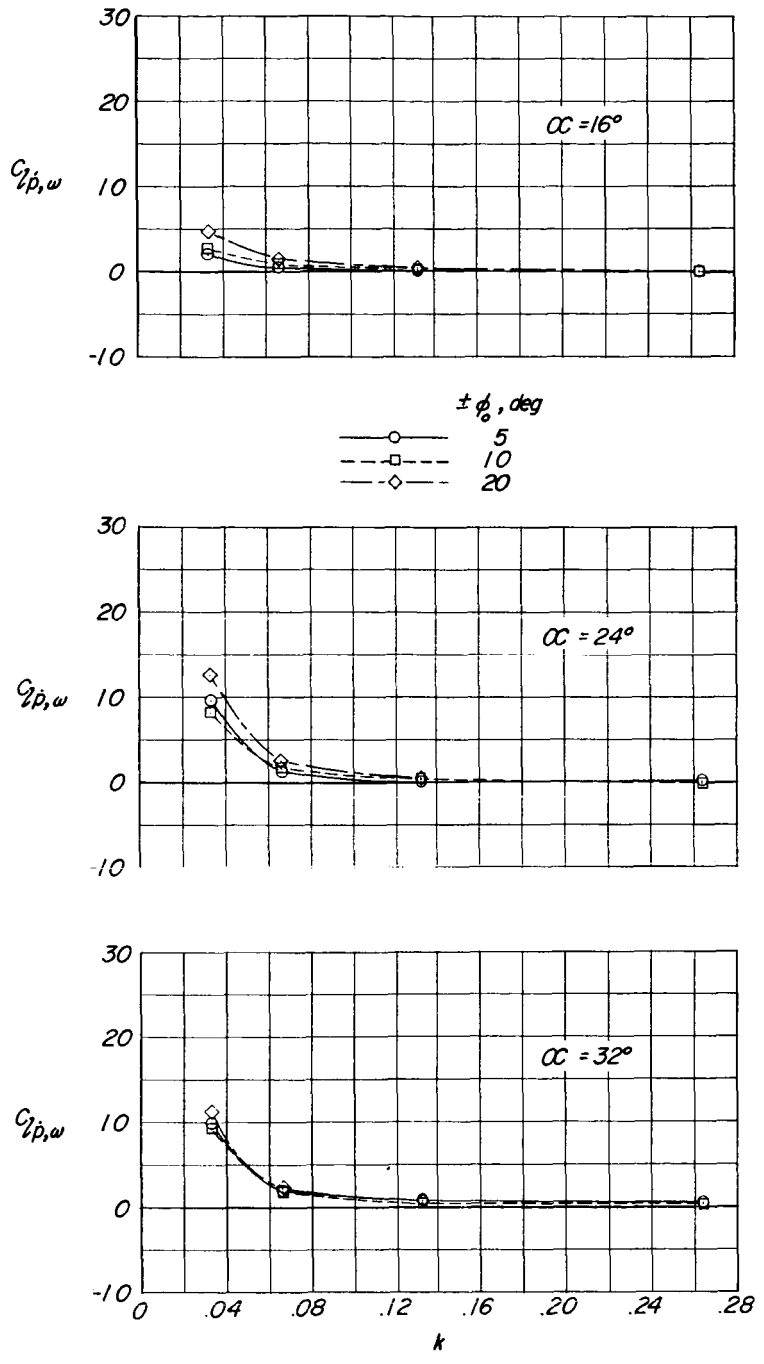

(c) Wing, fuselage, and tail.

Figure 13.- Concluded.

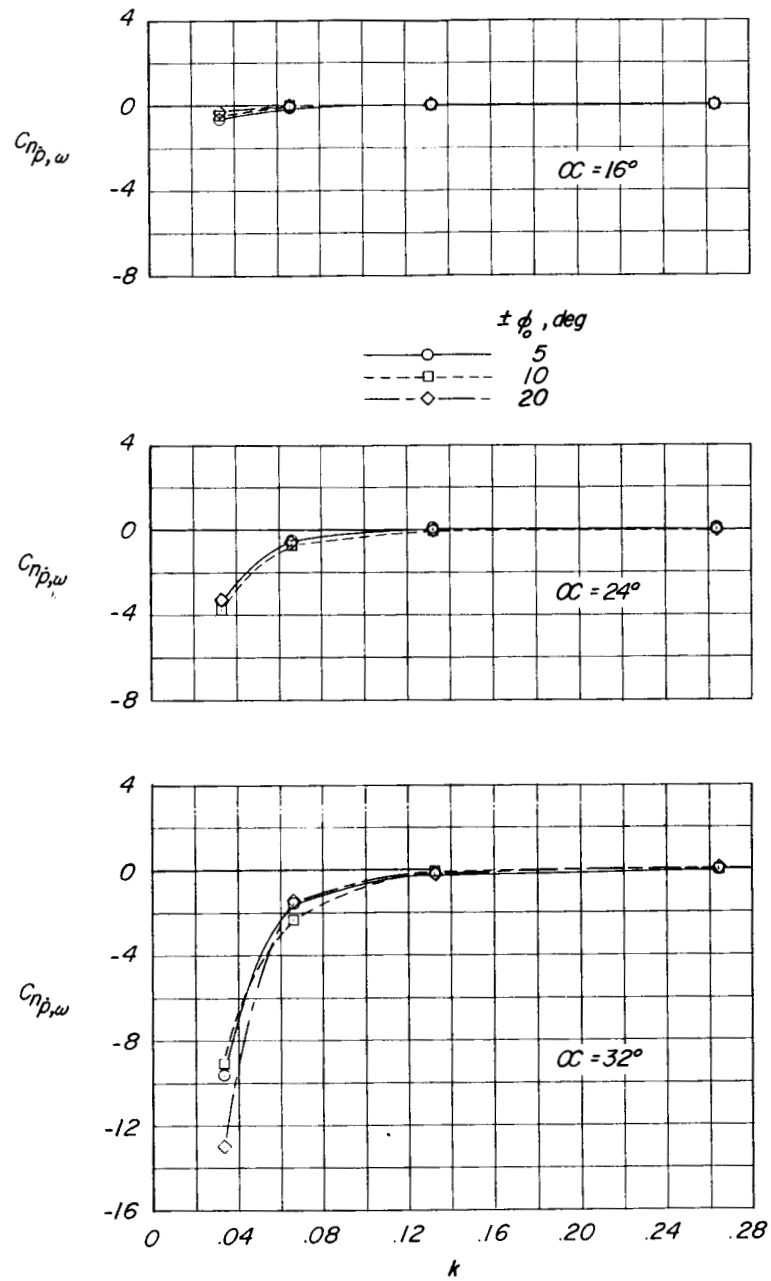

(a) Wing alone.

Figure 14.- The yawing moment due to rolling acceleration as a function of reduced frequency of oscillation for three high angles of attack.

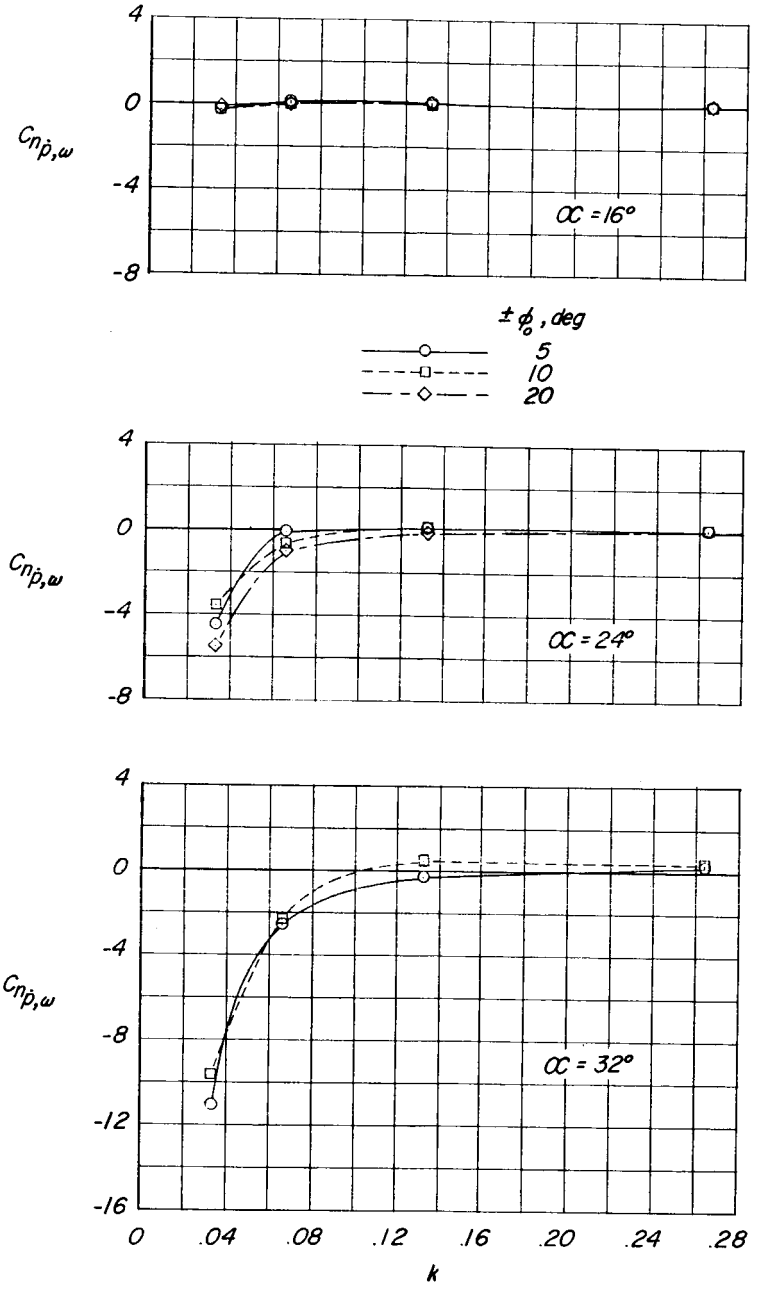

(b) Wing and fuselage.

Figure 14.- Continued.

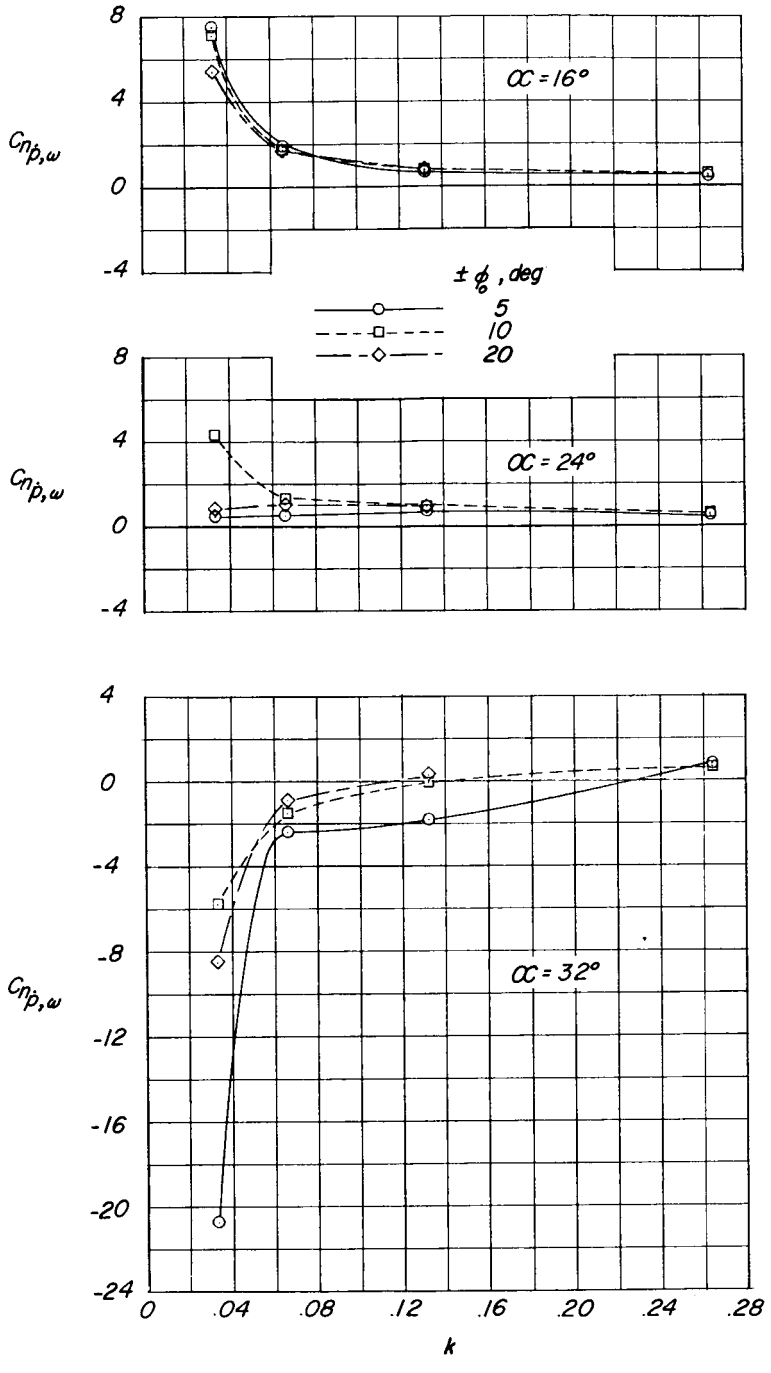

(c) Wing, fuselage, and tail.

Figure 14.- Concluded.

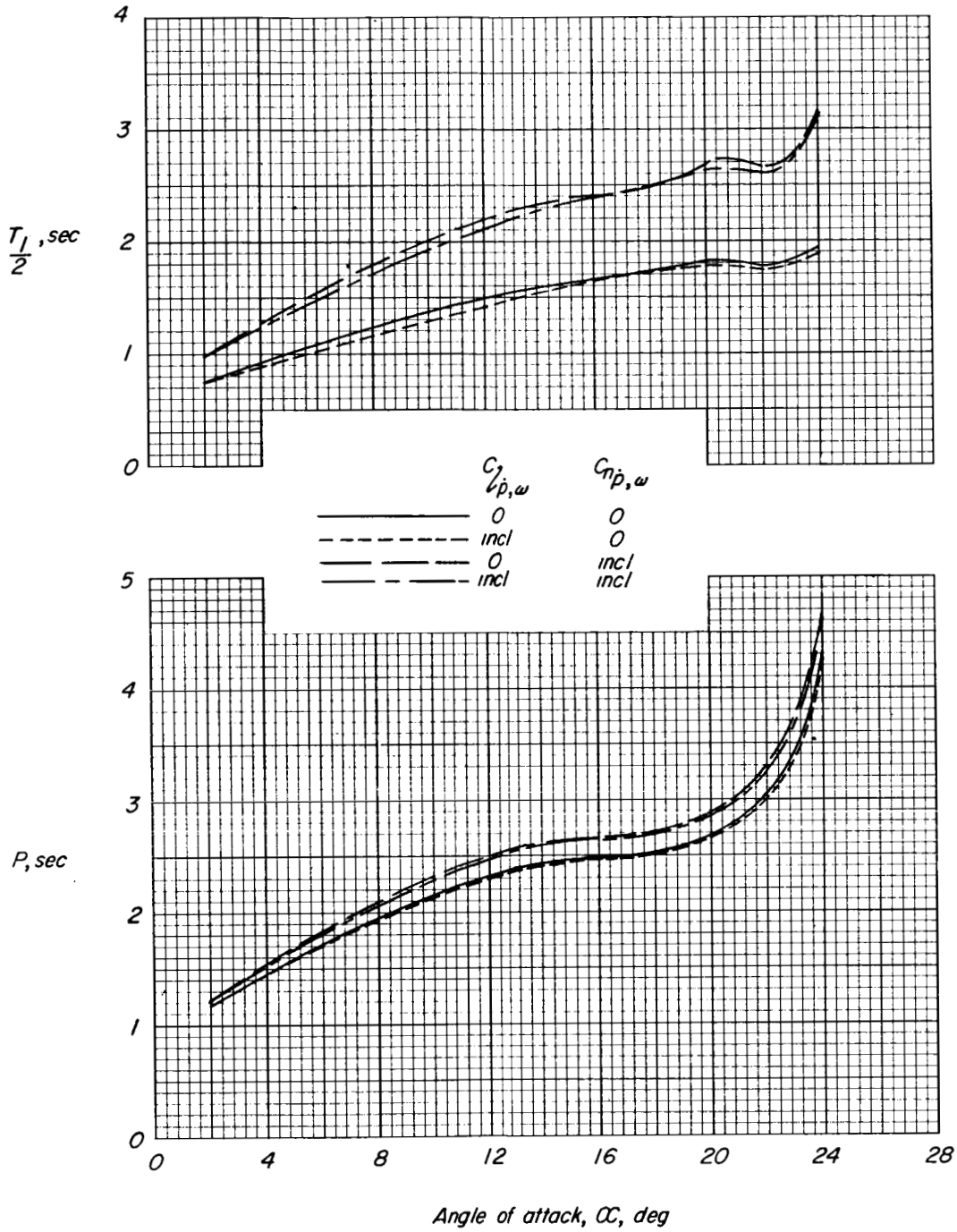

Figure 15.- Period and time to damp for a typical delta-wing airplane. The designation "Incl" signifies that this derivative was included in equations of motion for the computations.